buildings

MDPI

Article

Numerical Study and Design Method of Irregular Steel Beam-to-CFST Column Joints with Inclined Internal Diaphragms

Peng Li [1], Jialiang Jin [2,*], Yue Sheng [3], Wei Wang [2], Weifeng Jiao [1] and Tingting Gou [1]

[1] China Construction First Group Corporation Limited, Beijing 100071, China; lipeng@chinaonebuild.com (P.L.); jiaoweifeng@chinaonebuild.com (W.J.); goutingting@chinaonebuild.com (T.G.)
[2] State Key Laboratory of Disaster Reduction in Civil Engineering, Tongji University, Shanghai 200092, China; weiwang@tongji.edu.cn
[3] Pinghu City Construction Investment Corporation Limited, Jiaxing 314299, China; Shengy@phorg.com
* Correspondence: jialiangjin@tongji.edu.cn

Abstract

With the increasing functional and geometric complexity of modern steel buildings, irregular beam-to-column joints are becoming increasingly common in engineering practice, while their seismic performance and force transfer mechanisms remain insufficiently understood. Based on previous full-scale cyclic loading tests on unequal-depth steel beam (UDSB) and staggered steel beam (SSB) joints incorporating inclined internal diaphragms, this study presents numerical simulations and parametric analyses of irregular steel beam to concrete-filled steel tube (CFST) column joints. Three-dimensional nonlinear finite element models were developed using ABAQUS and validated against experimental results. The strengthening effects of internal diaphragms and concrete infill were then comparatively investigated. The results indicate that internal diaphragms increase the initial stiffness and load-carrying capacity of the joints to approximately 2.0–2.3 times and 1.16–1.8 times, respectively, compared with joints without diaphragms, whereas concrete infill provides smaller enhancements of about 1.3 times in stiffness and 1.2–1.3 times in strength. In addition, the hysteretic response of joints without diaphragms shows good agreement with the post-fracture behavior observed in the experiments, validating the diaphragm fracture mechanism. A parametric study further demonstrates that, under cyclic loading, the beam depth ratio, staggered floor ratio, column wall thickness, column width, diaphragm thickness, and diaphragm opening diameter have significant influences on joint strength and stress distribution, while the effect of axial load ratio is relatively minor. Finally, a strength prediction method applicable to inclined-diaphragm UDSB and SSB joints is proposed, and corresponding fitted expressions are derived based on the parametric results. The findings provide useful guidance for the seismic design of irregular steel beam–CFST column joints incorporating internal diaphragms.

Keywords: beam-to-column joint; staggered beam; unequal-depth beam; CFST column; internal diaphragm; seismic performance

Check for updates

Academic Editor: Antonio Formisano

Received: 1 March 2026
Revised: 5 April 2026
Accepted: 9 April 2026
Published: 11 April 2026

Copyright: © 2026 by the authors. Licensee MDPI, Basel, Switzerland. This article is an open access article distributed under the terms and conditions of the Creative Commons Attribution (CC BY) license.

1. Introduction

Concrete-filled steel tube (CFST) structures have been widely adopted in modern building engineering due to their high load-carrying capacity, favorable ductility, excellent seismic performance, and construction efficiency [1]. By combining the advantages of steel tubes and infilled concrete, CFST members can provide enhanced stiffness, strength, and energy dissipation capacity while maintaining relatively compact cross-sections [2–5].

Owing to these advantages, CFST columns have been increasingly used in high-rise and large-span steel structures, especially in systems requiring both structural efficiency and architectural flexibility.

Although CFST members exhibit excellent structural performance, the behavior of beam-to-column connections remains a critical issue in the design and assessment of CFST frame systems [6,7]. Under seismic loading, the joint region serves as the key zone for force transfer between beams and columns, and its mechanical behavior directly affects joint strength, stiffness, ductility, and overall structural reliability. This issue becomes more challenging in irregular beam-to-column joints (Figure 1), such as unequal-depth steel beam (UDSB) joints and staggered steel beam (SSB) joints, which are increasingly encountered in buildings with unequal story heights, staggered floors, transfer layouts, and other architecturally complex configurations. Compared with conventional symmetric joints, such irregular connections exhibit pronounced geometric asymmetry and nonuniform force transfer paths. As a result, their joint panel zones are subjected to more complex stress states and are more prone to stress concentration, out-of-plane deformation, and localized damage under seismic loading, posing challenges to reliable performance evaluation and rational design [8–10].

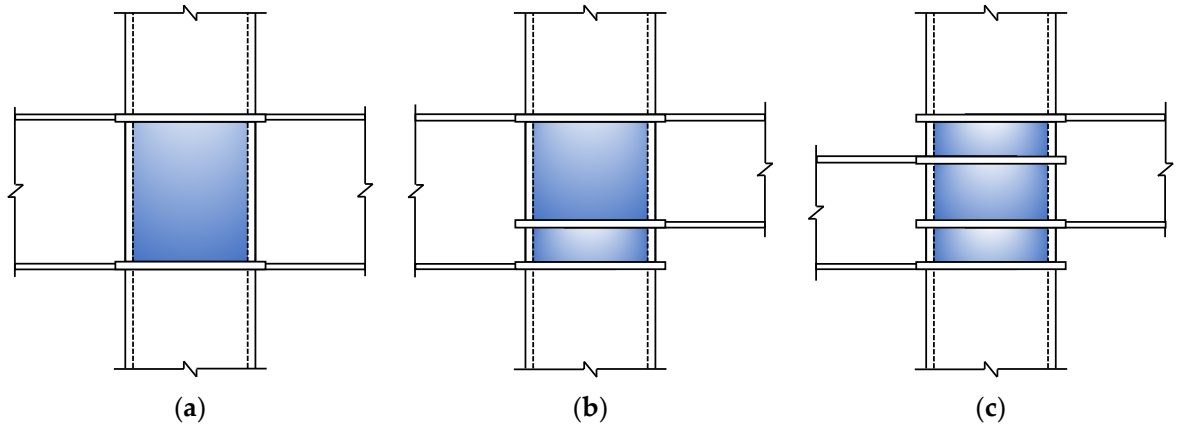

Figure 1. Standard and irregular beam-to-column joints. (**a**) Standard beam-to-column joint, (**b**) unequal-depth beam joint, (**c**) staggered beam joint.

Previous studies have shown that the mechanical behavior of irregular joints is strongly influenced by geometric asymmetry and local joint details. For UDSB joints, existing research has mainly focused on the effects of beam depth difference, joint configuration, and axial load level on stiffness, strength, and restoring force characteristics [11–17]. For hollow steel section (HSS) or CFST column joints, several strengthening details have been proposed to improve force transfer efficiency. For example, Mou et al. [18,19] and Sui et al. [20] developed outer annular stiffener-reinforced UDSB joints and established shear strength models for the joint panel zone considering the influence of beam depth ratio based on cyclic loading tests. Jin et al. [21] further proposed an insert-diaphragm UDSB joint for CFST columns and investigated its mechanical behavior through full-scale testing, numerical simulation, parametric analysis, and theoretical calculation.

Compared with UDSB joints, studies on SSB joints are relatively limited. Imai et al. [22] conducted monotonic loading tests on H-section beam-to-H-section column joints and revealed the influence of joint eccentricity on nonlinear restoring behavior. Kuwahara et al. [23] subsequently investigated the stiffness and strength characteristics of staggered beam joints with square steel tube columns. Liu et al. [24,25] reported through cyclic loading tests that SSB joints generally exhibit inferior hysteretic behavior, ductility, and energy dissipation capacity compared with conventional symmetric joints. Based on quasi-static

tests and finite element (FE) analysis, Sui et al. [10] studied circular steel tube column-to-H-section beam SSB joints and showed that the staggered height significantly affects initial stiffness, while its influence on shear strength is relatively limited.

Despite these efforts, systematic studies on irregular steel beam-to-CFST column joints remain insufficient, particularly for cases involving both geometric irregularity and diaphragm-assisted force transfer mechanisms. Existing studies often focused on specific joint details or individual parameters, whereas the combined effects of geometric proportions, diaphragm configuration, and concrete infill on joint behavior have not been fully clarified. In addition, conventional internal diaphragm solutions for irregular joints typically require multiple horizontal diaphragms arranged at different beam flange levels, which may lead to considerable fabrication difficulty, welding complexity, and quality control challenges in HSS or CFST columns with limited internal space [26–29]. To address these limitations, previous experimental research proposed an inclined internal diaphragm (IID) configuration for irregular steel beam-to-CFST column joints and validated its seismic performance through full-scale cyclic loading tests [30]. By introducing a single inclined diaphragm between the beam flanges, the proposed configuration can improve force transfer efficiency while simplifying the internal detailing compared with conventional multi-diaphragm arrangements [30]. However, the effects of key geometric and diaphragm-related parameters on the strength and stress distribution of such joints have not yet been systematically quantified, and a design-oriented strength prediction method is still lacking.

Based on the previous experimental study in Ref. [30], this paper presents a further numerical and theoretical investigation on irregular steel beam-to-CFST column joints with IIDs. Three-dimensional nonlinear FE models are first developed and validated for both UDSB and SSB joints under cyclic loading. On this basis, the strengthening effects of the internal diaphragms and concrete infill are comparatively examined. Subsequently, the influences of beam depth ratio, staggered height ratio, column wall thickness, column width, diaphragm thickness, diaphragm opening diameter, and axial load ratio on joint strength and stress distribution are systematically evaluated. Finally, based on the identified force transfer mechanisms between the inclined diaphragm, column wall, and beam ends, a strength prediction method for inclined-diaphragm UDSB and SSB joints is proposed, together with corresponding parametric fitting expressions.

2. Overview of Experimental Study

A previously conducted experimental study on irregular steel beam-to-CFST column joints with IIDs is briefly summarized in this section to provide the basis for FE model validation. Detailed descriptions of the experimental program can be found in the authors' earlier work [30]. Two full-scale beam-to-column joint subassemblies were tested under cyclic loading, including one unequal-depth beam (UDB) joint and one staggered beam (SB) joint, as shown in Figure 2. Both specimens employed square CFST columns with cross-sectional dimensions of 300 × 300 × 10 mm, filled with self-compacting C45 concrete. The UDB specimen used two welded H-section beams with different depths, while the SB specimen adopted beams of the same section with a vertical offset between beam elevations. The key geometric parameters are summarized in Table 1.

The overall test configuration and loading scheme are illustrated in Figure 3. Cyclic vertical displacements were applied at the beam ends in an antisymmetric manner, while a constant axial compressive force was maintained on the column. The loading protocol was displacement-controlled in terms of story drift ratio, following AISC 341-22 [31].

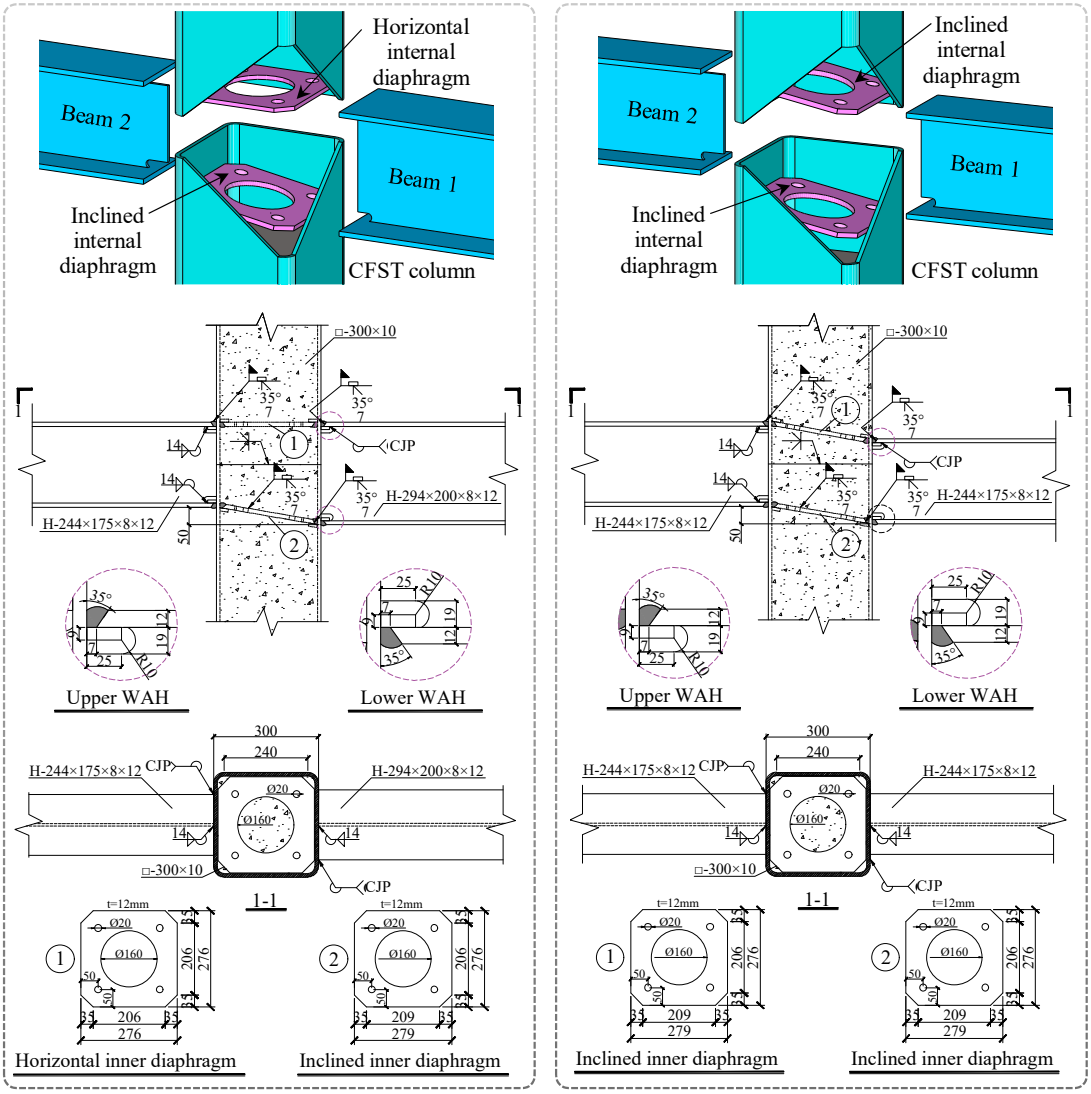

Figure 2. Details and schematic layout of test specimens (unit: mm). (**a**) UDSB specimen (UDSBJ-IID-1), (**b**) SSB specimen (SSBJ-IID-1).

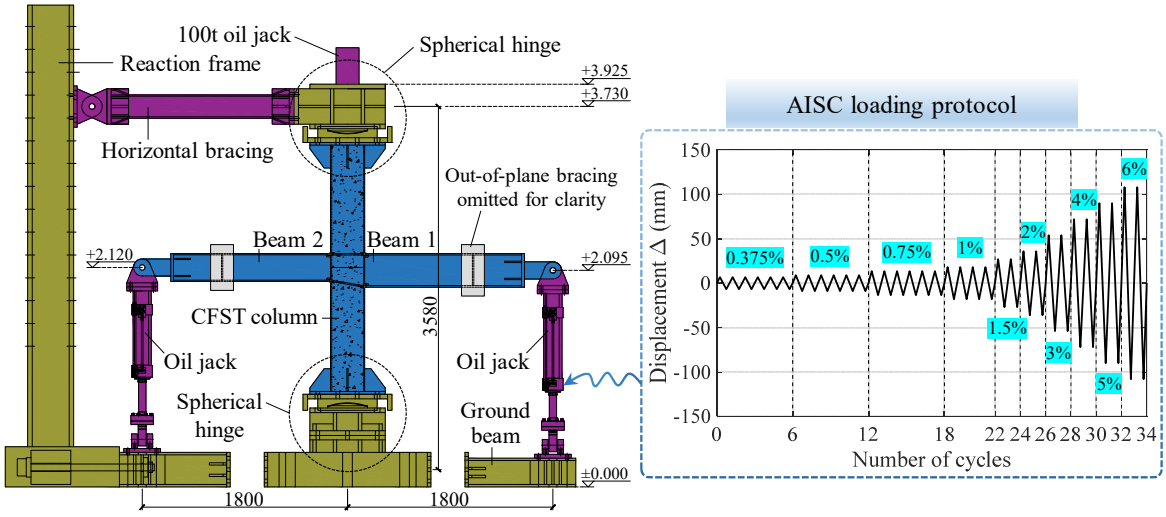

Figure 3. Overall view of test setup (unit: mm).

Table 1. Geometric properties of the specimens.

Specimen	Steel Column (mm)	Beam 1 (mm)	Beam 2 (mm)	H_2/H_1	ΔH (mm)
UDSBJ-IID-1	HSS-300 × 300 × 10	H-294 × 200 × 8 × 12	H-244 × 175 × 8 × 12	0.83	-
SSBJ-IID-1		H-244 × 175 × 8 × 12		1.00	50

3. Finite Element Simulation

3.1. Finite Element Modeling

Three-dimensional nonlinear FE models of irregular steel beam-to-CFST column joints with IIDs were developed in ABAQUS 6.14 [32] based on the previously tested specimens in Ref. [30]. Figure 4 illustrates the specifics of the FE modeling. All structural components, including steel beams, square steel tube columns, internal diaphragms, and infilled concrete, were modeled using eight-node reduced-integration solid elements (C3D8R). A mesh sensitivity study was conducted by assigning five different element sizes in the joint region, namely 40 mm, 30 mm, 20 mm, 15 mm, and 10 mm, as shown in Figure 5. The assessment considered the global hysteretic response, the predicted peak force, and the corresponding computational cost. As shown in Figure 5a, the hysteretic curves gradually converge as the mesh is refined. Figure 5b further indicates that the predicted peak force approaches the test result with decreasing mesh size, while the difference between the 15 mm and 10 mm meshes becomes small. Meanwhile, Figure 5c shows that the computational cost increases markedly for finer meshes, especially from 15 mm to 10 mm. Considering both accuracy and efficiency, a multi-scale meshing strategy was adopted, with a 15 mm mesh in the joint core region, a 30 mm transition mesh, and a 50 mm mesh in regions away from the connection. This strategy provides sufficient accuracy for capturing the joint response while maintaining reasonable computational cost.

Reference points were defined at the beam ends and column ends and coupled to the corresponding end surfaces to apply loading and boundary conditions. The column ends were modeled as pinned, cyclic vertical displacements were imposed at the beam ends, and a constant axial compressive force was applied at the column top.

The interaction between steel and concrete components was explicitly considered to simulate composite action and force transfer within the joint. Surface-to-surface contact was defined between the steel tube and the infilled concrete, as well as between the diaphragm and the concrete core. A hard contact formulation was adopted in the normal direction to prevent penetration, while tangential behavior was modeled using a penalty-based friction law. According to relevant studies [33,34], the coefficient of friction at the steel-concrete interface decreases with the increase in relative interfacial displacement, and the friction coefficient generally ranges from 0.3 to 0.5. Therefore, the friction coefficient in this study was taken as 0.3, following previous studies on CFST/CFSST members and steel–concrete interfaces [21,30,33–36]. Welded steel-to-steel interfaces were modeled using tie constraints.

Steel materials subjected to low-cycle reversed loading exhibit pronounced Bauschinger and ratcheting effects, accompanied by cyclic hardening or softening behavior. Isotropic hardening describes only yield surface expansion, whereas kinematic hardening accounts for yield surface translation but fails to represent cyclic hardening saturation. The Chaboche combined isotropic–kinematic hardening model [37], incorporating both mechanisms, is therefore adopted to simulate the cyclic plastic behavior of structural steel. Based on material coupon tests, a combined hardening model employing the von Mises yield criterion and associated flow rule was used for Q355B steel. Steel components were modeled using a multi-linear elastic-plastic constitutive relationship calibrated from the previous experimental study [38]. In the ABAQUS implementation, the kinematic hardening component was introduced through the combined hardening model using the half-cycle stress-plastic strain

data with three backstresses, while the isotropic hardening evolution in the ABAQUS *cyclic hardening* option was further determined following the method proposed by Hai et al. [39]. The two key parameters adopted in this study were Q_∞ = 70.15 MPa and b = 12.95, where Q_∞ denotes the saturation value of isotropic hardening and b controls the rate at which the hardening variable evolves toward saturation. A comparison between the combined hardening model and conventional isotropic hardening is presented in Figure 6.

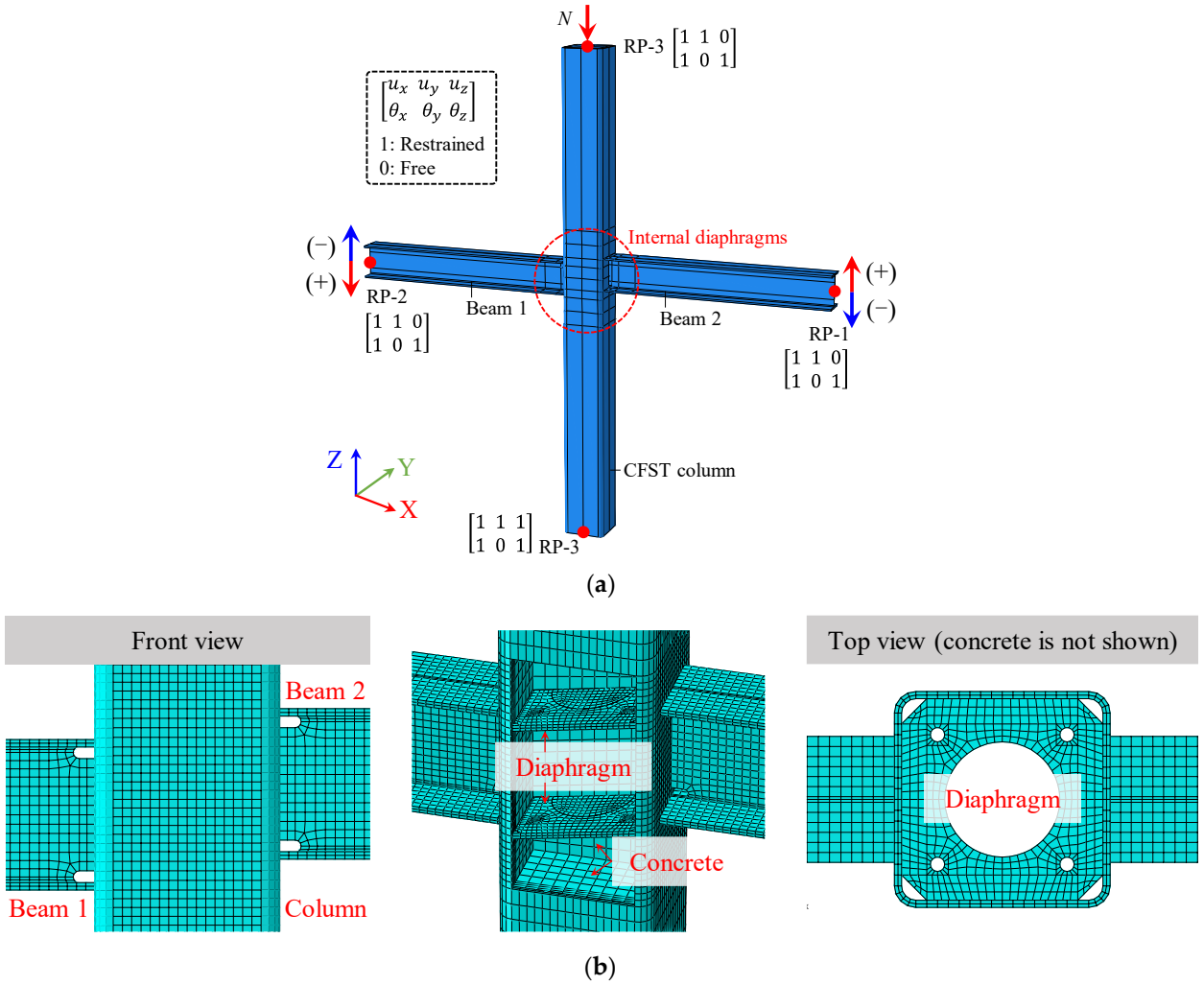

Figure 4. Details of the FE model (SSB joint). (**a**) Boundary conditions, (**b**) mesh generation.

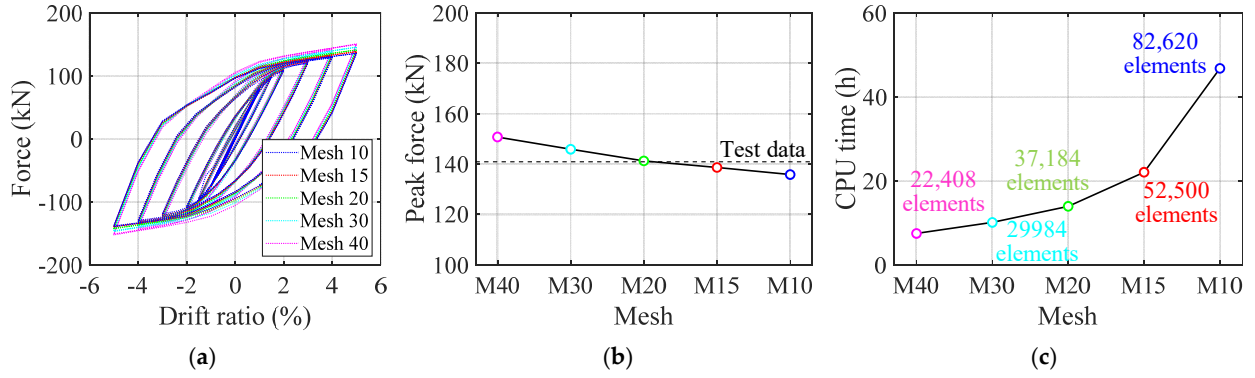

Figure 5. Mesh sensitivity analysis. (**a**) Hysteretic curves, (**b**) peak force, (**c**) comparison of CPU time.

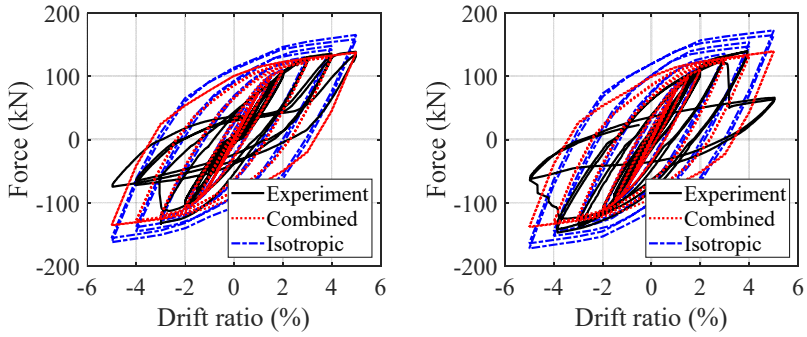

Figure 6. Validation of the combined hardening model. (**a**) Specimen UDSBJ-IID-1, (**b**) specimen SSBJ-IID-1.

The nonlinear behavior of the infilled concrete was simulated using the concrete damaged plasticity (CDP) model available in ABAQUS [32]. The plasticity parameters of the CDP model were calibrated based on material tests [30]: dilation angle $\Psi = 35°$, flow potential eccentricity $e = 0.1$, biaxial-to-uniaxial compressive strength ratio $f_{b0}/f_{c0} = 1.16$, $K = 0.667$, and viscosity parameter = 0.05. The remaining constitutive details of the concrete model, including the compressive and tensile relations and the associated damage definitions, followed the previously published study [30].

3.2. Validation of FE Models

Figures 7 and 8 present comparisons between the improved FE models and the experimental results for specimens UDSBJ-IID-1 and SSBJ-IID-1, respectively. Figures 7a and 8a show the relationships between beam-end force and drift ratio, including the hysteretic and backbone curves. Although strength degradation was observed in the experiments at drift ratios of approximately 3–4% due to fracture of the internal diaphragms, the FE-predicted hysteretic responses exhibit good agreement with the test results in terms of overall shape, characteristic behavior, and stiffness degradation trends. For both UDSBJ-IID-1 and SSBJ-IID-1, the initial stiffness and peak strength predicted by the FE models closely match the experimental values, with discrepancies of less than 5%.

Figures 7b and 8b compare the experimentally observed ultimate failure modes with those obtained from the FE analyses. The numerical models successfully capture the joint response prior to fracture and clearly identify stress concentration regions at the beam flange–column wall interfaces and the diaphragm–column connections, which correspond well to the fracture locations observed in the tests. Pronounced stress concentrations are also observed in the steel tube and the infilled concrete near the joint panel zone. Although the FE models do not explicitly reproduce steel fracture or material separation, they effectively represent the critical stress transfer paths, localized deformation patterns, and the progressive stress concentration process leading to failure. These results demonstrate that the proposed FE models can reliably capture the fundamental mechanical response, stress concentration pattern, and force-transfer mechanism of the tested joints prior to diaphragm fracture, thus providing a sound basis for the subsequent parametric study and strength-oriented analysis. According to the experimental observations, diaphragm fracture occurred at drift ratios of approximately 3–5%, and this range may therefore be regarded as a practical reference for the applicable range of the present FE model. Since no explicit fracture criterion was incorporated, the model is not intended to predict the exact onset of diaphragm cracking or the post-fracture response. The corresponding limitations are further discussed in Section 6.

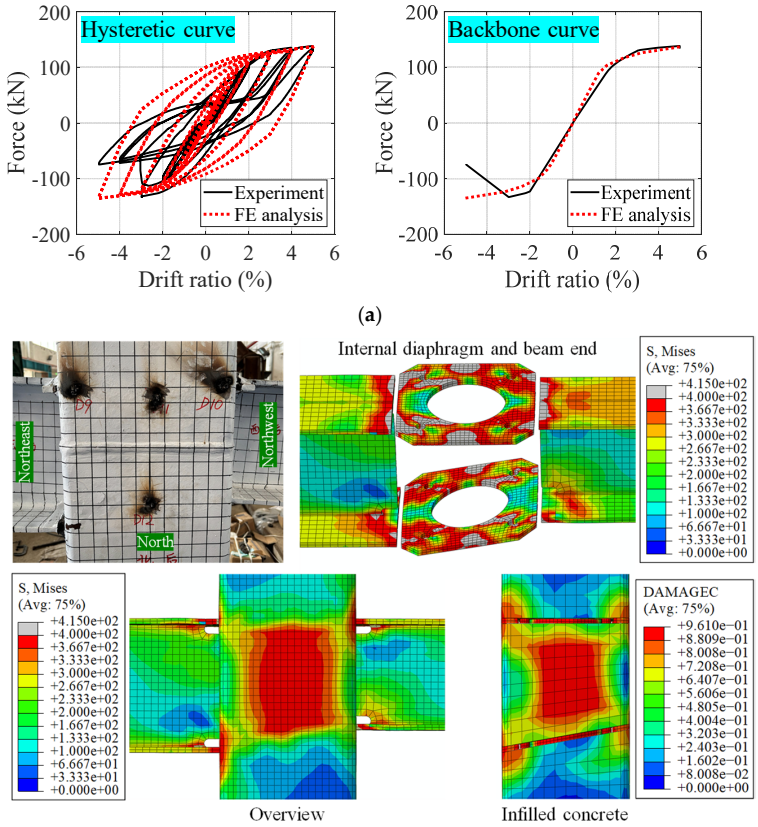

Figure 7. Comparative analysis of the FEM and the specimen UDSBJ-IID-1. (**a**) Comparison of the force-drift curves, (**b**) comparison of the ultimate failure modes.

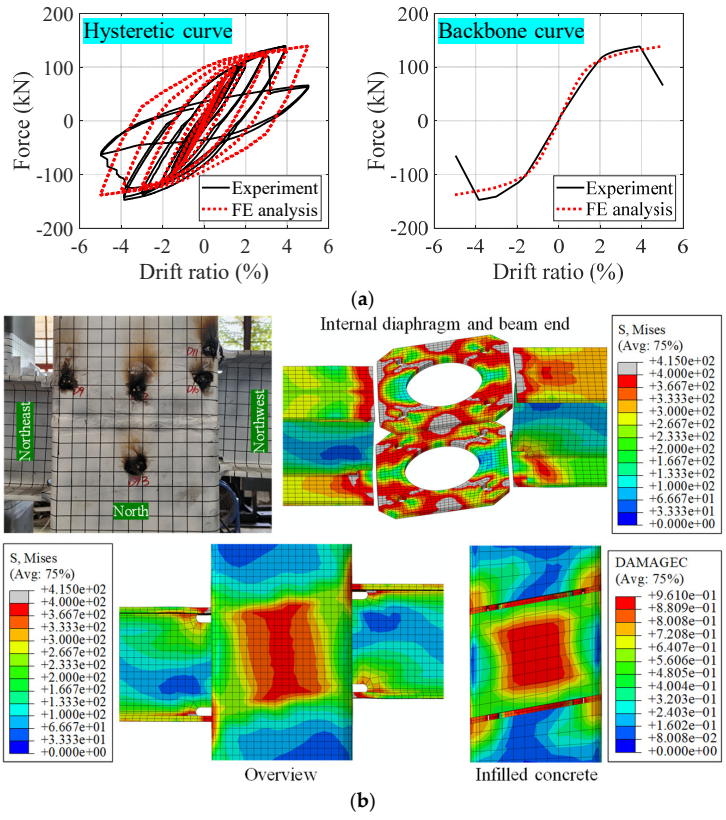

Figure 8. Comparative analysis of the FEM and the specimen SSBJ-IID-1. (**a**) Comparison of the force-drift curves, (**b**) comparison of the ultimate failure modes.

3.3. Strengthening Effect of Inclined Internal Diaphragms

To further clarify the role of the IID in irregular steel beam-to-CFST column joints, comparative FE models without internal diaphragms were established based on the validated modeling framework. Figure 9 compares the hysteretic responses of joints with and without internal diaphragms, together with the experimental results. As shown in Figure 9, the presence of the IID significantly improves the seismic response of both UDSBJ-IID-1 and SSBJ-IID-1. The initial stiffness of the joints with IIDs is approximately 1.6–1.8 times that of the corresponding joints without diaphragms, while the peak strength increases by about 2.0–2.3 times. In contrast, the joints without diaphragms exhibit markedly pinched hysteretic responses, lower initial stiffness, and earlier strength deterioration, indicating that the panel zone alone cannot provide an efficient and stable force transfer path under the irregular loading condition.

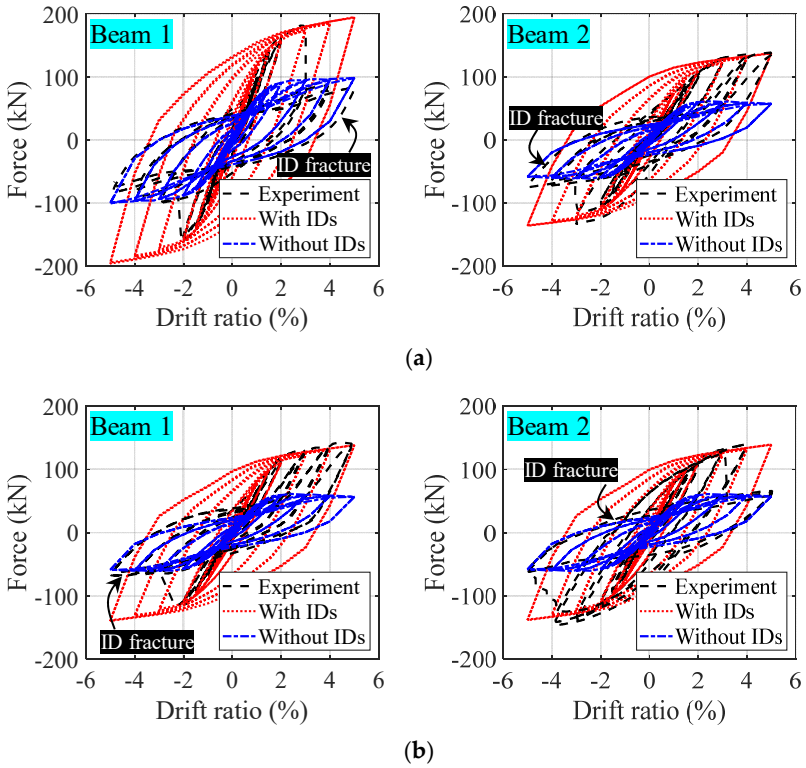

Figure 9. The strengthening effect of internal diaphragms. (**a**) Specimen UDSBJ-IID-1, (**b**) specimen SSBJ-IID-1.

When internal diaphragms are provided, the joints can maintain higher load levels and fuller hysteretic responses over a wider drift range, indicating improved energy dissipation capacity and deformation compatibility. Although diaphragm fracture occurred in the experiments at drift ratios of approximately 3–4%, causing localized strength reduction, the numerical results show that the overall hysteretic response after fracture remains markedly superior to that of the joints without diaphragms. This indicates that the IID plays a dominant strengthening role during the early and intermediate loading stages, and its beneficial influence does not vanish immediately after local fracture.

From a mechanical perspective, the IID serves as the primary load-resisting component in the proposed joint configuration. It provides a more direct transmission path for the beam flange forces to the column wall, thereby reducing stress concentration and out-of-plane demand in the panel zone. This role is particularly important for irregular joints, where the beam-end forces are vertically misaligned due to unequal beam depths or staggered elevations. Under such geometric asymmetry, the IID helps redistribute the internal force

flow and improves deformation compatibility between the upper and lower parts of the joint region.

The novelty of the proposed detail lies in the use of a single inclined diaphragm to connect the force-transfer paths associated with irregular beam flanges, instead of relying on multiple horizontal diaphragms arranged at different elevations. In this way, the proposed configuration can improve joint resistance and force-transfer efficiency while maintaining a more rational internal load path for irregular geometry.

From a practical viewpoint, the proposed IID still requires proper fabrication and concrete placement control within the joint zone. However, compared with conventional irregular joints using multiple horizontal diaphragms at different beam-flange levels, the single inclined diaphragm provides a simpler internal arrangement and is more suitable for square steel tube columns with relatively large cross-sections, which is beneficial for practical fabrication and construction.

3.4. Strengthening Effect of Concrete Infill

To evaluate the contribution of concrete infill, additional FE models without infilled concrete were developed and compared with the corresponding filled-joint models. The comparative hysteretic responses are shown in Figure 10. The results indicate that concrete infill has a positive but more moderate effect on joint behavior than the IID. For both UDSBJ-IID-1 and SSBJ-IID-1, the initial stiffness of the filled joints is approximately 1.3 times that of the unfilled joints, while the peak strength increases by about 1.2–1.3 times. Compared with the unfilled models, the infilled joints exhibit steeper initial loading slopes and higher load levels at small drift ratios, demonstrating that concrete infill effectively enhances the initial stiffness and strength of the joint panel zone.

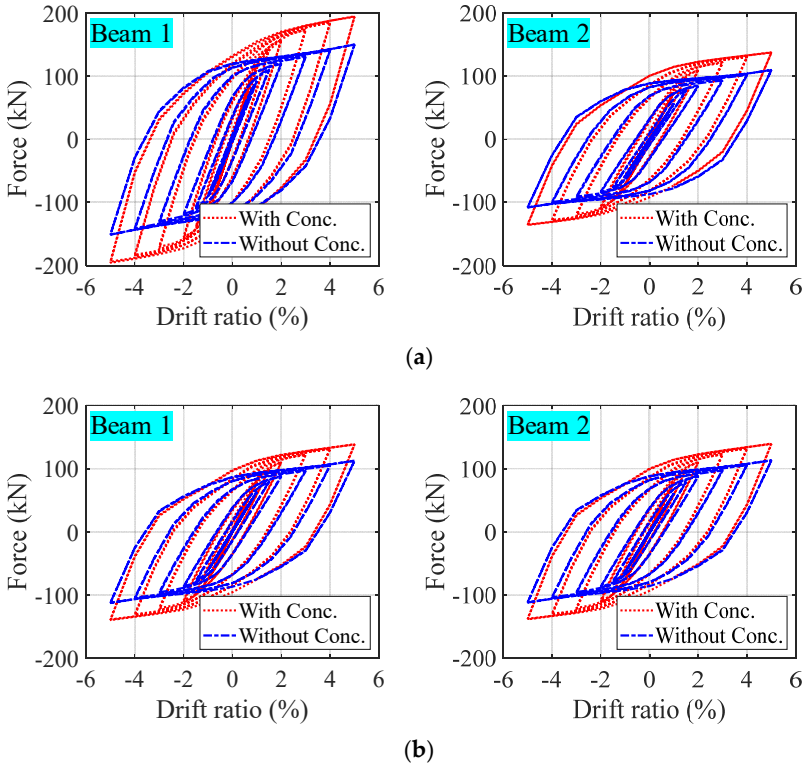

Figure 10. The strengthening effect of infill concrete. (**a**) Specimen UDSBJ-IID-1, (**b**) specimen SSBJ-IID-1.

Mechanically, the concrete infill mainly plays a secondary and complementary role. Unlike the IID, which directly participates in the transfer of beam flange forces, the concrete

core primarily enhances the confinement and local stability of the steel tube and contributes to stress redistribution within the joint zone. It can also share part of the compressive and shear demand in the panel region, thereby improving initial rigidity and delaying local deterioration. However, its influence on the global hysteretic envelope and peak resistance remains less pronounced than that of the IID.

These results indicate that the seismic improvement of the proposed irregular joint is governed mainly by the diaphragm-assisted steel force-transfer mechanism, while the concrete infill provides beneficial support through confinement and local stress moderation. In other words, the IID is the dominant strengthening component, whereas the concrete infill acts as a supplementary component that enhances the stability and robustness of the joint response.

4. Parametric Analysis

4.1. Parameter Design

To identify the governing parameters affecting the mechanical behavior of UDSB and SSB joints incorporating internal diaphragms, a systematic parametric study was performed based on the validated FE modeling framework. A series of FE models were constructed by independently varying key geometric parameters while keeping other conditions unchanged. The detailed parameter combinations of all numerical models are summarized in Tables 2 and 3.

Table 2. Parameters for FE models of the UDSB joints.

Model	Column (mm)	Beam 1 (mm)	Beam 2 (mm)	H_2/H_1	t_c (mm)	D_c (mm)	t_d (mm)	R (mm)	n
UDSB-1	300 × 300 × 10	244 × 175 × 8 × 12	294 × 175 × 8 × 12	0.83	10	300	12	160	0.15
UDSB-2	300 × 300 × 10	244 × 175 × 8 × 12	394 × 175 × 8 × 12	0.62	10	300	12	160	0.15
UDSB-3	300 × 300 × 10	244 × 175 × 8 × 12	494 × 175 × 8 × 12	0.49	10	300	12	160	0.15
UDSB-4	300 × 300 × 10	244 × 175 × 8 × 12	594 × 175 × 8 × 12	0.41	10	300	12	160	0.15
UDSB-5	300 × 300 × 6	244 × 175 × 8 × 12	294 × 175 × 8 × 12	0.83	6	300	12	160	0.15
UDSB-6	300 × 300 × 8	244 × 175 × 8 × 12	294 × 175 × 8 × 12	0.83	8	300	12	160	0.15
UDSB-7	300 × 300 × 12	244 × 175 × 8 × 12	294 × 175 × 8 × 12	0.83	12	300	12	160	0.15
UDSB-8	300 × 300 × 14	244 × 175 × 8 × 12	294 × 175 × 8 × 12	0.83	14	300	12	160	0.15
UDSB-9	200 × 200 × 10	244 × 175 × 8 × 12	294 × 175 × 8 × 12	0.83	10	200	12	160	0.15
UDSB-10	250 × 250 × 10	244 × 175 × 8 × 12	294 × 175 × 8 × 12	0.83	10	250	12	160	0.15
UDSB-11	350 × 350 × 10	244 × 175 × 8 × 12	294 × 175 × 8 × 12	0.83	10	350	12	160	0.15
UDSB-12	400 × 400 × 10	244 × 175 × 8 × 12	294 × 175 × 8 × 12	0.83	10	400	12	160	0.15
UDSB-13	300 × 300 × 10	244 × 175 × 8 × 12	294 × 175 × 8 × 12	0.83	10	300	10	160	0.15
UDSB-14	300 × 300 × 10	244 × 175 × 8 × 12	294 × 175 × 8 × 12	0.83	10	300	14	160	0.15
UDSB-15	300 × 300 × 10	244 × 175 × 8 × 12	294 × 175 × 8 × 12	0.83	10	300	16	160	0.15
UDSB-16	300 × 300 × 10	244 × 175 × 8 × 12	294 × 175 × 8 × 12	0.83	10	300	12	120	0.15
UDSB-17	300 × 300 × 10	244 × 175 × 8 × 12	294 × 175 × 8 × 12	0.83	10	300	12	140	0.15
UDSB-18	300 × 300 × 10	244 × 175 × 8 × 12	294 × 175 × 8 × 12	0.83	10	300	12	180	0.15
UDSB-19	300 × 300 × 10	244 × 175 × 8 × 12	294 × 175 × 8 × 12	0.83	10	300	12	160	0
UDSB-20	300 × 300 × 10	244 × 175 × 8 × 12	294 × 175 × 8 × 12	0.83	10	300	12	160	0.4
UDSB-21	300 × 300 × 10	244 × 175 × 8 × 12	294 × 175 × 8 × 12	0.83	10	300	12	160	0.6

The investigated parameters and their corresponding ranges are as follows:

(1) Beam depth ratio for UDSB joints (H_2/H_1): 0.41, 0.49, 0.62, and 0.83.
(2) Staggered floor ratio for SSB joints ($\Delta H/H_1$): 0.2 (ΔH = 50 mm), 0.4 (ΔH = 100 mm), 0.6 (ΔH = 150 mm), and 0.8 (ΔH = 200 mm).
(3) Column wall thickness (t_c): 6, 8, 10, 12, and 14 mm.
(4) Column width (D_c): 200, 250, 300, 350, and 400 mm.
(5) Diaphragm thickness (t_d): 10, 12, 14, and 16 mm.
(6) Diaphragm opening diameter (R): 120, 140, 160, and 180 mm.
(7) Axial load ratio (n): 0, 0.15, 0.4, and 0.6.

Table 3. Parameters for FE models of the SSB joints.

Model	Column (mm)	Beam 1/Beam 2 (mm)	$\Delta H/H_1$	t_c (mm)	D_c (mm)	t_d (mm)	R (mm)	n
SSB-1	300 × 300 × 10	244 × 175 × 8 × 12	0.2	10	300	12	160	0.15
SSB-2	300 × 300 × 10	244 × 175 × 8 × 12	0.4	10	300	12	160	0.15
SSB-3	300 × 300 × 10	244 × 175 × 8 × 12	0.6	10	300	12	160	0.15
SSB-4	300 × 300 × 10	244 × 175 × 8 × 12	0.8	10	300	12	160	0.15
SSB-5	300 × 300 × 6	244 × 175 × 8 × 12	0.2	6	300	12	160	0.15
SSB-6	300 × 300 × 8	244 × 175 × 8 × 12	0.2	8	300	12	160	0.15
SSB-7	300 × 300 × 12	244 × 175 × 8 × 12	0.2	12	300	12	160	0.15
SSB-8	300 × 300 × 14	244 × 175 × 8 × 12	0.2	14	300	12	160	0.15
SSB-9	200 × 200 × 10	244 × 175 × 8 × 12	0.2	10	200	12	160	0.15
SSB-10	250 × 250 × 10	244 × 175 × 8 × 12	0.2	10	250	12	160	0.15
SSB-11	350 × 350 × 10	244 × 175 × 8 × 12	0.2	10	350	12	160	0.15
SSB-12	400 × 400 × 10	244 × 175 × 8 × 12	0.2	10	400	12	160	0.15
SSB-13	300 × 300 × 10	244 × 175 × 8 × 12	0.2	10	300	10	160	0.15
SSB-14	300 × 300 × 10	244 × 175 × 8 × 12	0.2	10	300	14	160	0.15
SSB-15	300 × 300 × 10	244 × 175 × 8 × 12	0.2	10	300	16	160	0.15
SSB-16	300 × 300 × 10	244 × 175 × 8 × 12	0.2	10	300	12	120	0.15
SSB-17	300 × 300 × 10	244 × 175 × 8 × 12	0.2	10	300	12	140	0.15
SSB-18	300 × 300 × 10	244 × 175 × 8 × 12	0.2	10	300	12	180	0.15
SSB-19	300 × 300 × 10	244 × 175 × 8 × 12	0.2	10	300	12	160	0
SSB-20	300 × 300 × 10	244 × 175 × 8 × 12	0.2	10	300	12	160	0.4
SSB-21	300 × 300 × 10	244 × 175 × 8 × 12	0.2	10	300	12	160	0.6

In the following parametric study, the joint behavior is assessed mainly by the yield force, peak force, and stress distribution. The yield and peak forces are extracted from the backbone curve of each model, and the yield point is defined using the equivalent energy method shown in Figure 11.

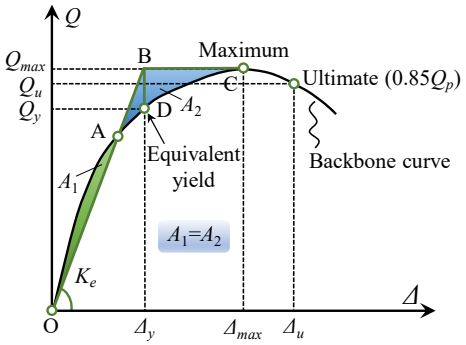

Figure 11. Definition of key performance points.

4.2. Influence of Beam Depth Ratio (H_2/H_1)

With the beam depth on one side fixed at H_2 = 244 mm, a parametric analysis was conducted for beam depth ratios H_2/H_1 = 0.41, 0.49, 0.62, and 0.83. The corresponding cyclic responses and stress distributions of the UDSB joints are presented in Figure 12. The results indicate that the beam depth ratio has a pronounced influence on the cyclic behavior and force redistribution of the joint.

Figure 12a illustrates the hysteretic responses on the Beam 1 side, together with the variations in yield strength and peak strength on both the Beam 1 and Beam 2 sides. As the beam depth ratio increases, the hysteresis loops on the Beam 1 side progressively expand and exhibit a fuller shape, accompanied by a significant increase in enclosed area. This trend indicates notable enhancements in load-carrying capacity and energy dissipation on the deeper beam side. In contrast, the load-carrying capacity on the Beam 2 side gradually decreases with increasing beam depth ratio. Quantitatively, compared with the model with H_2/H_1 = 0.41, the peak shear capacity of Beam 1 increases by 42.3%, 85.2%, and 129.8% for H_2/H_1 = 0.49, 0.62, and 0.83, respectively. Meanwhile, the peak shear capacity of Beam 2 decreases by 3.0%, 5.3%, and 8.6%, respectively. This asymmetric response reflects the

redistribution of internal forces within the joint, whereby a larger proportion of the load is attracted to the deeper beam, consequently suppressing the force demand on the shallower beam. This result indicates that the beam depth ratio does not merely affect the strength level, but fundamentally governs the internal force allocation and asymmetric resistance development of UDSB joints.

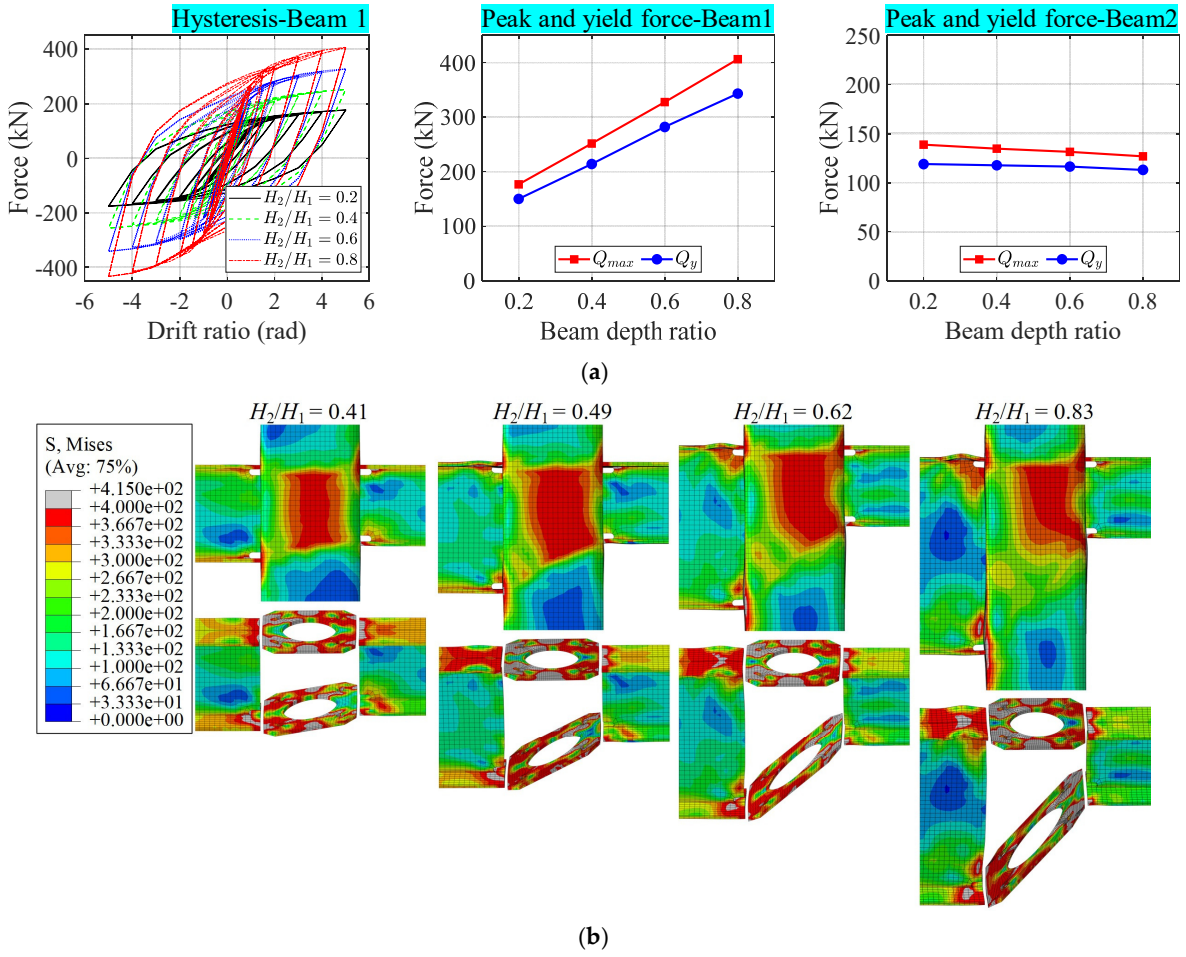

Figure 12. Influence of beam depth ratio on UDSB joints. (**a**) Force response of the joint, (**b**) stress distribution of the joint.

Figure 12b shows the evolution of stress distributions within the joint as the beam depth ratio increases. It can be observed that higher beam depth ratios lead to more severe stress concentrations in the joint region. On the shallower beam side, stresses gradually shift from the column wall toward the inclined internal diaphragm, whereas on the deeper beam side, pronounced stress concentrations develop at the beam flange–column wall interface and at the diaphragm–column wall connection. Excessively large beam depth ratios therefore tend to accelerate damage initiation at the deeper beam-to-column interface. From a design perspective, this indicates that overly large beam depth ratios should be avoided, and that appropriate matching between beam depth ratio, diaphragm configuration, and column wall thickness is essential to prevent premature local failure.

4.3. Influence of Staggered Floor Ratio ($\Delta H/H_1$)

Under otherwise identical geometric and material conditions, a parametric study was conducted on SSB joints with staggered floor ratios $\Delta H/H_1$ of 0.2, 0.4, 0.6, and 0.8. The corresponding force responses and stress distributions are presented in Figure 13.

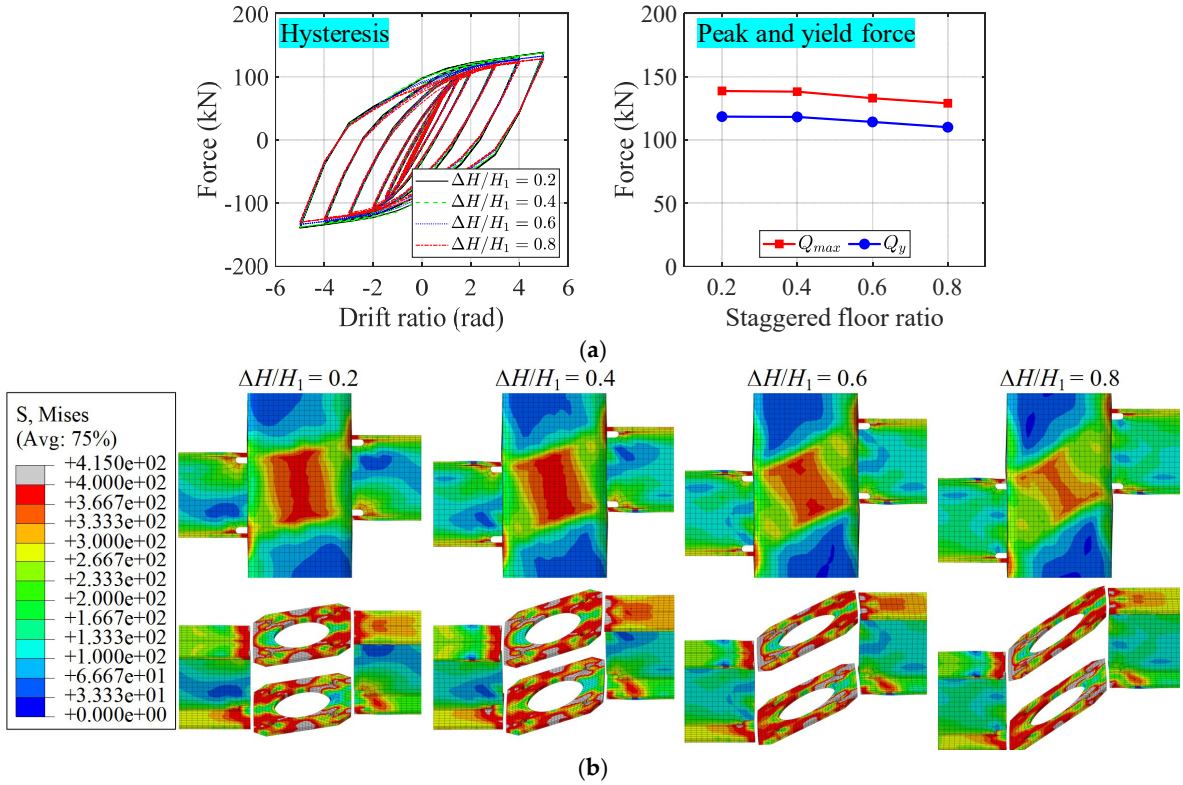

Figure 13. Influence of staggered floor ratio on SSB joints. (**a**) Force response of the joint, (**b**) stress distribution of the joint.

Figure 13a shows the hysteretic responses as well as the variations in yield and peak strengths for different staggered floor ratios. As the hysteretic responses of the two beams were essentially identical, only the results of Beam 1 are reported. As $\Delta H/H_1$ increases, the hysteresis loops become slightly less full, accompanied by a gradual reduction in both yield strength and peak load capacity. Nevertheless, no pronounced pinching behavior is observed within the investigated range, indicating that the inclined internal diaphragm remains effective in maintaining stable force transfer and satisfactory deformation compatibility even under large staggered configurations. Quantitatively, compared with the joint with $\Delta H/H_1$ = 0.2, the peak load capacity decreases by approximately 0.4%, 4.1%, and 7.0% when $\Delta H/H_1$ increases to 0.4, 0.6, and 0.8, respectively. The overall reduction remains moderate, suggesting that the adverse effect of vertical eccentricity induced by staggered floors is controllable within the considered range. Therefore, within the investigated range, $\Delta H/H_1$ mainly acts as a geometric asymmetry parameter that influences local stress redistribution more than the global strength level.

Figure 13b illustrates the equivalent stress distributions of the joints with different staggered floor ratios. With increasing ΔH/H1, the overall stress level in the joint panel zone slightly decreases, while stress concentration gradually shifts toward the internal diaphragm and its connection to the column wall. For smaller staggered ratios, the stress distribution among the beam flanges, internal diaphragm, and column wall is relatively uniform, whereas larger staggered ratios amplify structural asymmetry and intensify local stress concentration at the diaphragm–column wall interface.

Overall, $\Delta H/H_1$ has a noticeable but limited influence on the hysteretic performance of IID SSB joints, mainly reflected by a slight reduction in load-carrying capacity and increased local stress concentration. From a design perspective, relatively large staggered floor ratios can still be accommodated provided that the diaphragm dimensions and column wall

thickness are properly designed, with particular attention given to the beam end on the staggered side and the diaphragm–column wall connection region.

4.4. Influence of Column Wall Thickness (t_c)

With all other geometric and material parameters kept constant, the column wall thickness was varied as t_c = 6, 8, 10, 12, and 14 mm to investigate its influence on the seismic behavior of both UDSB and SSB joints. The corresponding force-deformation responses and stress distributions are presented in Figures 14 and 15.

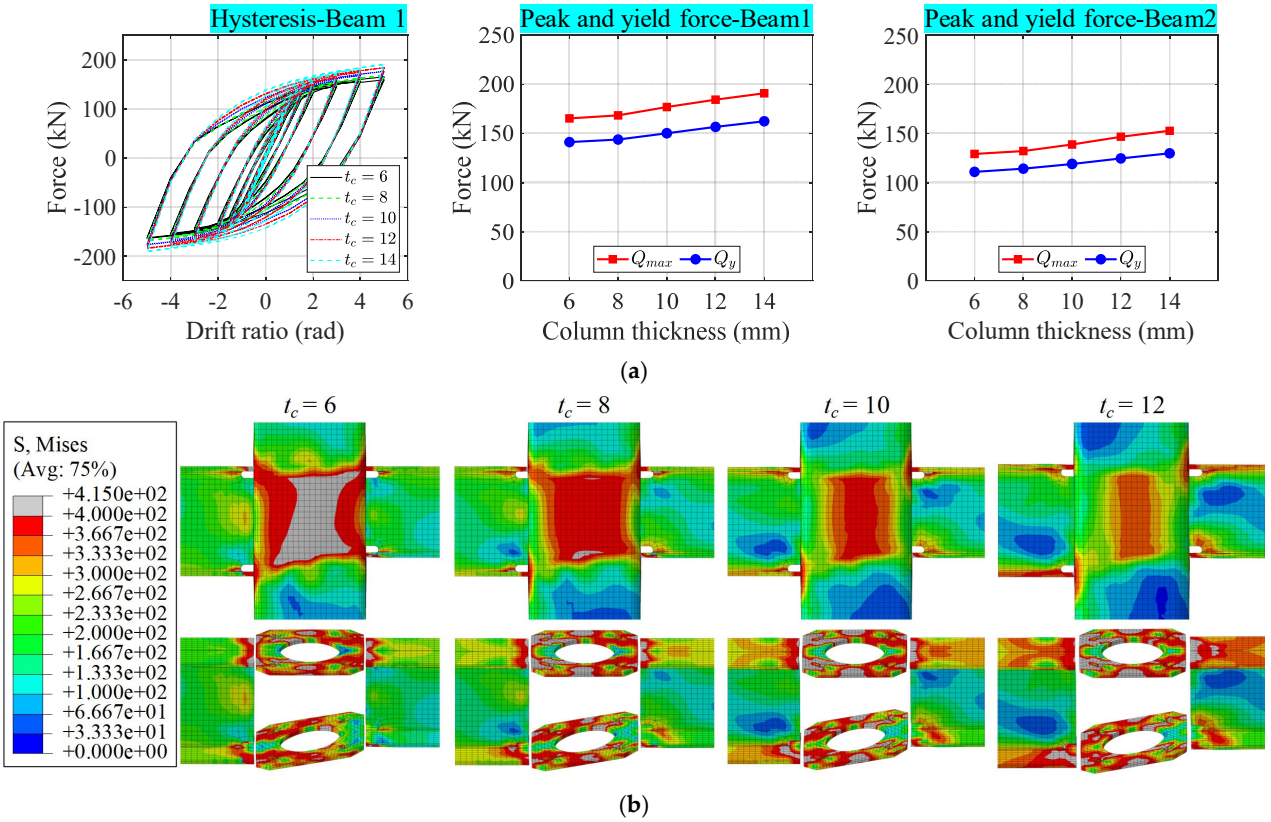

Figure 14. Influence of column wall thickness on UDSB joints. (**a**) Force response of the joint, (**b**) stress distribution of the joint.

Figures 14a and 15a show the hysteretic responses together with the variations in yield and peak strengths under different column wall thicknesses. It can be observed that, as t_c increases, the hysteresis loops of both UDSB and SSB joints gradually expand, accompanied by a consistent increase in yield strength and peak load capacity. In all cases, the hysteresis curves remain stable and full, without evident pinching behavior, indicating that increasing the column wall thickness effectively enhances the global stiffness and seismic resistance of the joints. Quantitatively, when the column wall thickness increases from 6 mm to 14 mm, the yield and peak strengths at both Beam 1 and Beam 2 exhibit an approximately linear growth trend. The peak load capacity of the UDSB and SSB joints is enhanced by about 15.6–18.2% and 23.1%, respectively, demonstrating the pronounced strengthening effect of column wall thickness on joint capacity. This indicates that the column wall thickness is a primary sectional parameter controlling the panel-zone stiffness and overall load-carrying capacity of both UDSB and SSB joints.

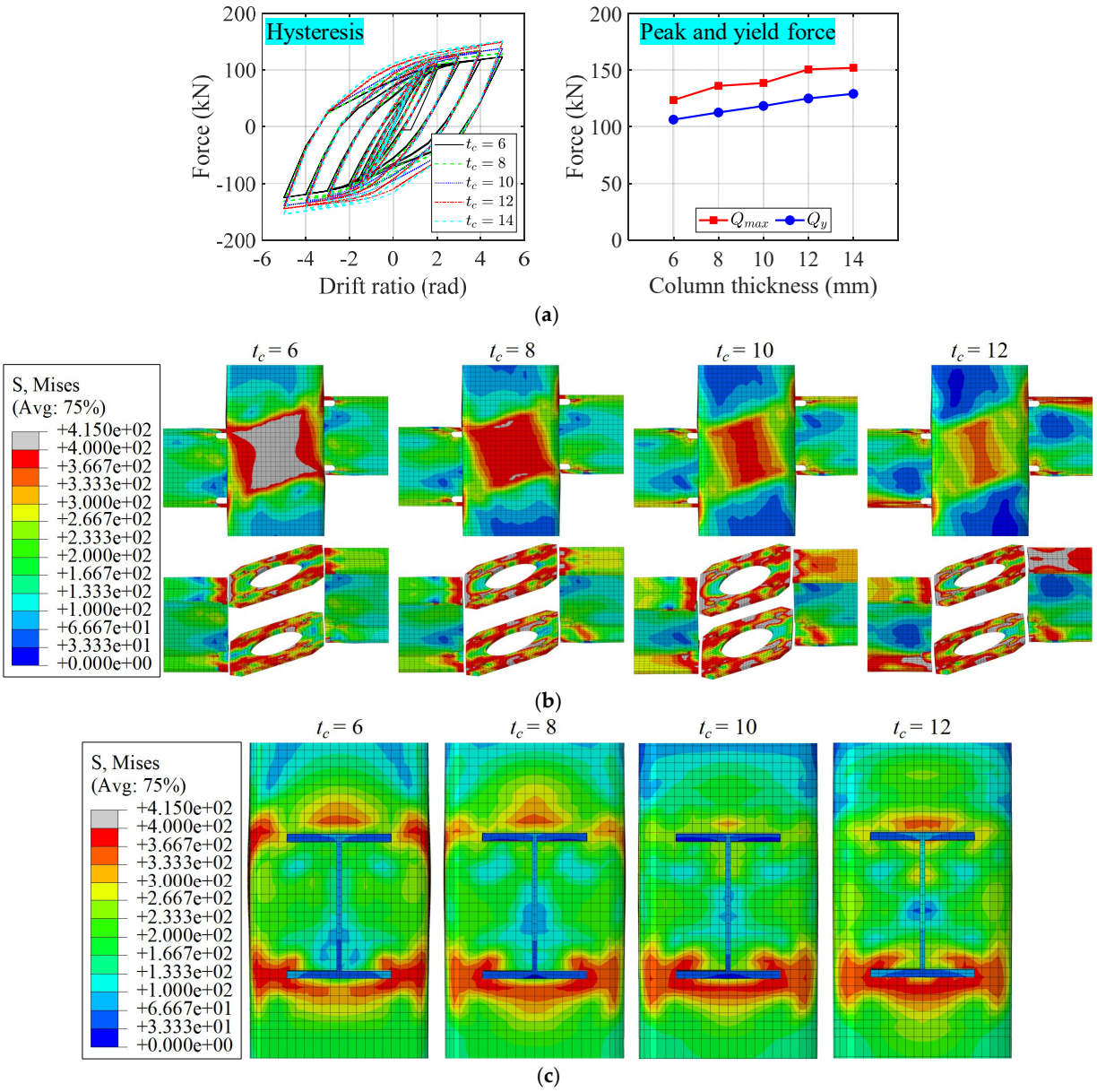

Figure 15. Influence of column wall thickness on SSB joints. (**a**) Force response of the joint; (**b**) stress distribution of the joint; (**c**) stress distribution of the frontal flange of the column.

Figures 14b and 15b illustrate the equivalent stress distributions of the joints for different column wall thicknesses. For relatively thin column walls (t_c = 6 mm), pronounced stress concentrations are observed in the column panel zone, particularly near the beam-to-column interfaces. As the column wall thickness increases, the overall stress level within the panel zone decreases and the stress distribution becomes more uniform. Meanwhile, higher stress demand gradually develops in the internal diaphragms and beam ends, indicating their increased participation in force transfer and a more rational and efficient load path within the joint. A similar trend is also observed in the frontal flange of the column (Figure 15c), where the local stress concentration near the beam-to-column interface is alleviated as the column wall thickness increases.

4.5. Influence of Column Width (D_c)

With all other geometric and material parameters kept constant, the column width was varied as D_c = 200, 250, 300, 350, and 400 mm to investigate its influence on the seismic

behavior of both UDSB and SSB joints. The corresponding force-deformation responses and stress distributions are presented in Figures 16 and 17.

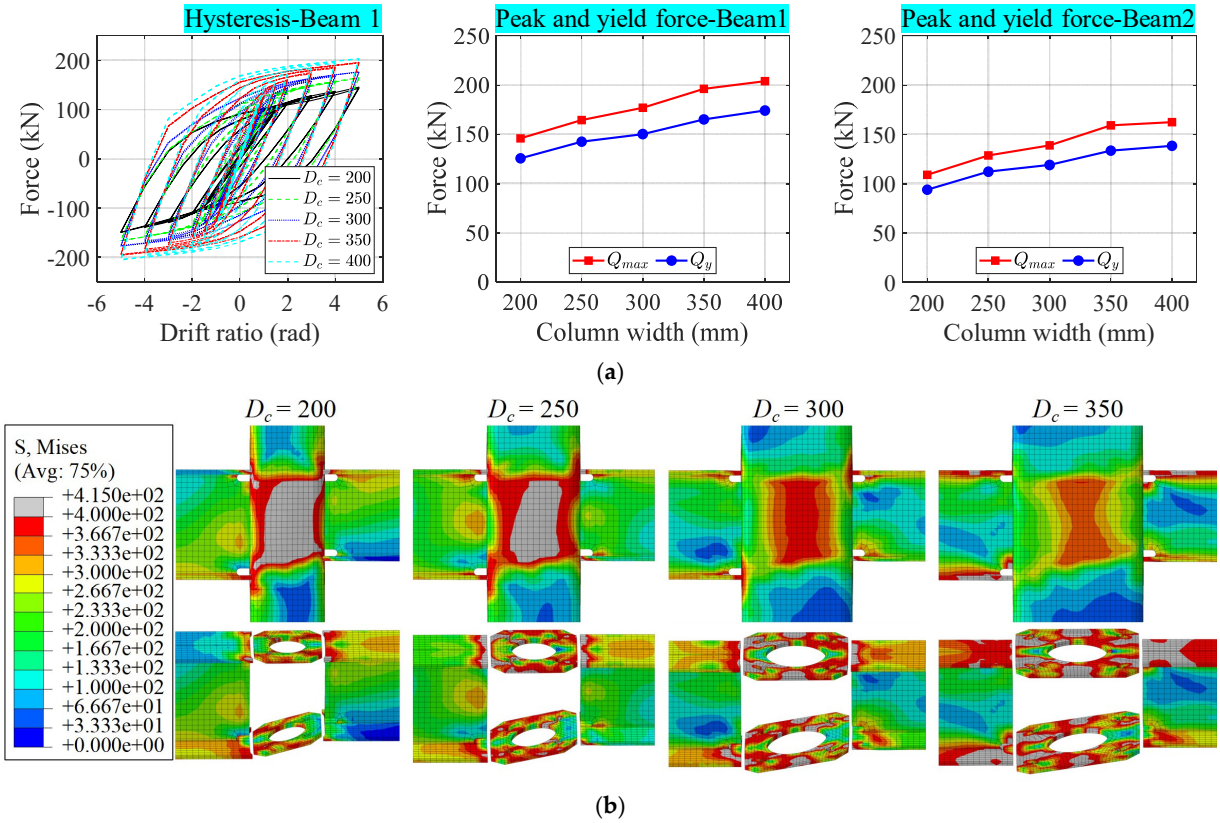

Figure 16. Influence of column width on UDSB joints. (**a**) Force response of the joint, (**b**) stress distribution of the joint.

Figures 16a and 17a show the hysteretic responses together with the variations in yield and peak strengths under different column widths. It can be observed that, as the column width D_c increases, the hysteresis loops of both UDSB and SSB joints gradually expand, accompanied by a continuous increase in yield strength and peak load capacity. In all cases, the hysteresis curves remain stable and full, without noticeable pinching behavior, indicating that increasing the column width effectively enhances the shear stiffness and load-carrying capacity of the joint panel zone, thereby improving the overall seismic performance of the joints. It is worth noting that the strengthening effect of column width exhibits a diminishing marginal benefit. Quantitatively, when the column width increases from 300 mm to 350 mm, the peak load capacity of the joints increases by approximately 10.8–16.5%. However, a further increase in column width from 350 mm to 400 mm results in a much smaller gain in peak strength, limited to about 2.1–4.0%. This indicates that, at larger column widths, the joint capacity is progressively governed by other components, such as the beam ends or internal diaphragms, and the contribution of further column widening becomes less pronounced. Therefore, although increasing D_c is beneficial to joint strength and panel-zone behavior, its strengthening effect shows a clear diminishing marginal benefit beyond a certain range.

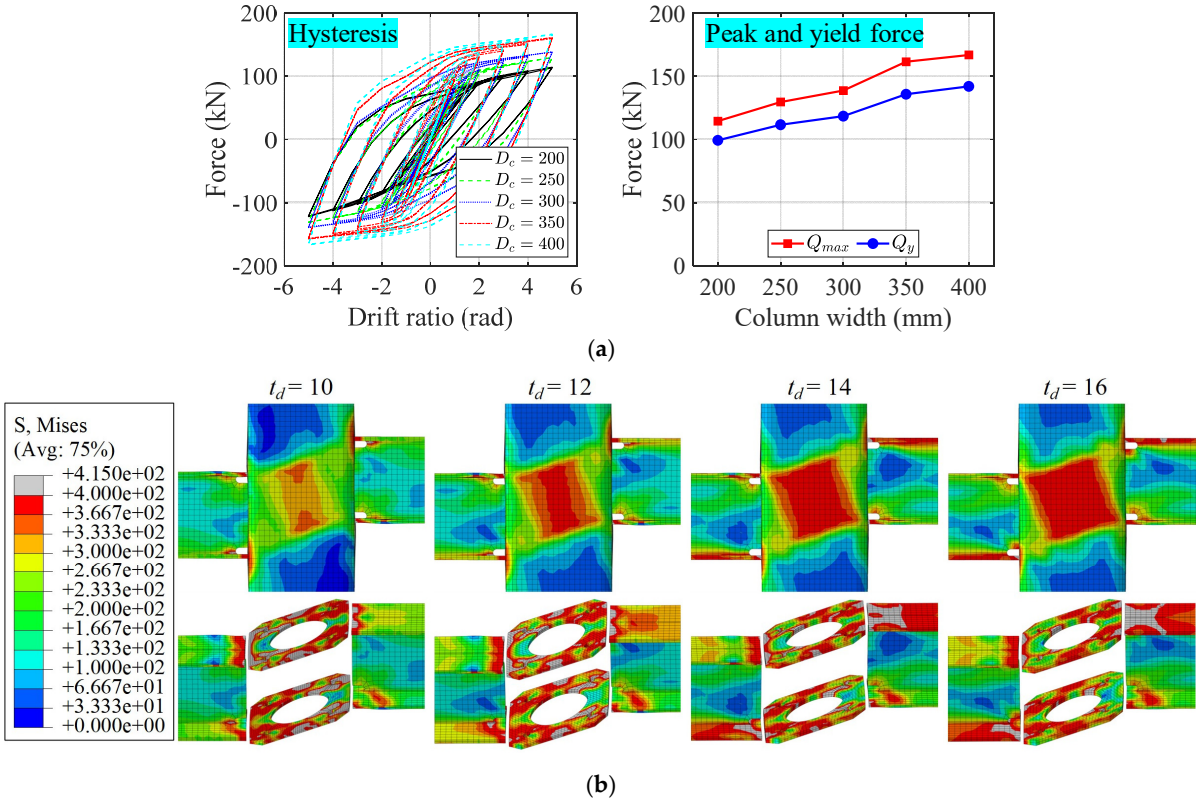

Figure 17. Influence of column width on SSB joints. (**a**) Force response of the joint, (**b**) stress distribution of the joint.

Figures 16b and 17b illustrate the equivalent stress distributions of the joints under different column widths. For relatively narrow columns (D_c = 200 mm), pronounced stress concentrations are observed in the column panel zone, particularly near the beam-to-column interfaces. As the column width increases, the stress distribution within the panel zone becomes more uniform, and the out-of-plane deformation of the column wall is effectively restrained. Meanwhile, higher stress demand develops in the beam ends and the internal diaphragm–column wall connections, indicating a clearer and more efficient force transfer path, with the internal diaphragms playing an increasingly significant role in shear force sharing.

Overall, column width is identified as an important parameter influencing the seismic performance of irregular steel beam–CFST column joints with inclined internal diaphragms. A moderate increase in column width can effectively enhance joint strength, stiffness, and stress distribution. However, excessive enlargement provides limited additional benefit. From a design perspective, the column width should be selected judiciously, considering both structural performance and material efficiency, to ensure adequate seismic safety of UDSB and SSB joints.

4.6. Influence of Diaphragm Thickness (t_d)

Keeping all other geometric and material parameters unchanged, a series of parametric analyses were conducted on UDSB and SSB joints by varying the diaphragm thickness as t_d = 10, 12, 14, and 16 mm. The corresponding mechanical responses and stress distributions are presented in Figures 18 and 19. Figures 18a and 19a illustrate the hysteretic responses of the joints together with the variations in yield and peak strengths under different diaphragm thicknesses.

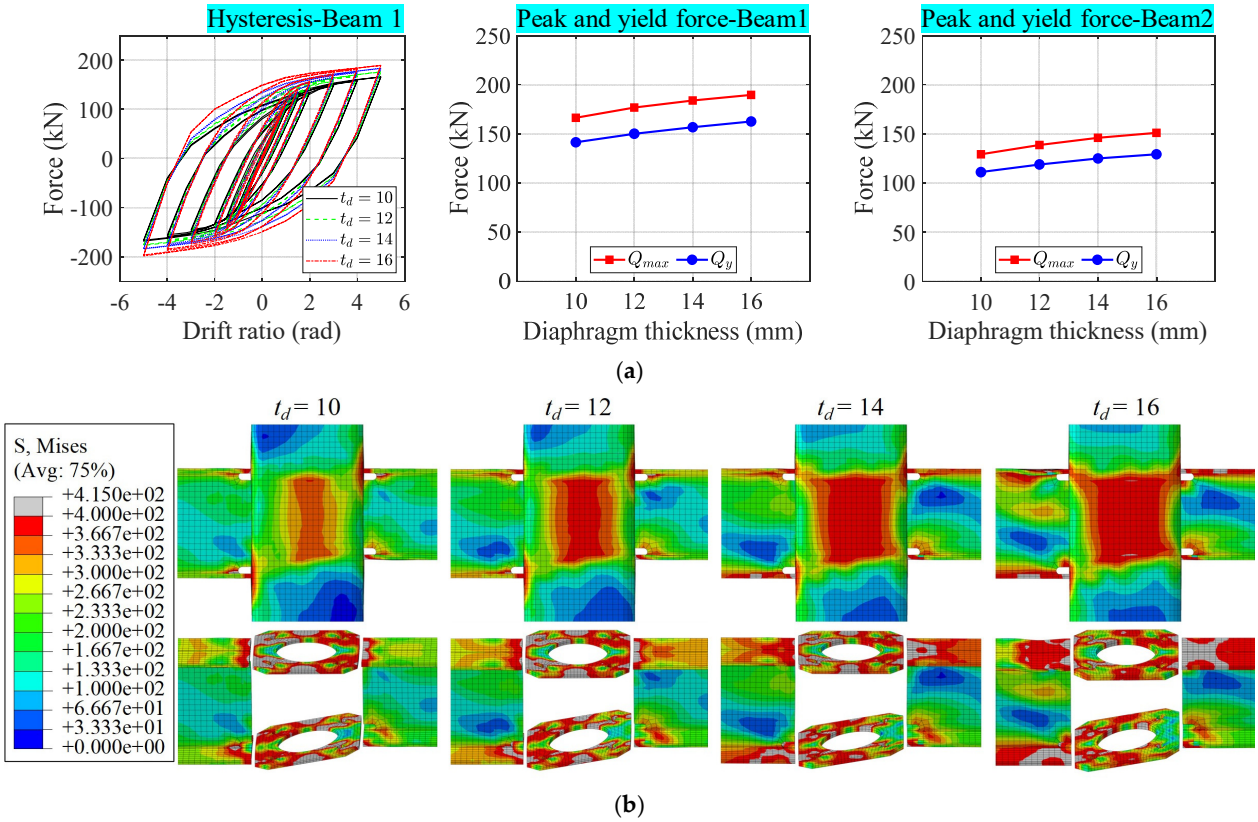

Figure 18. Influence of diaphragm thickness on UDSB joints. (**a**) Force response of the joint, (**b**) stress distribution of the joint.

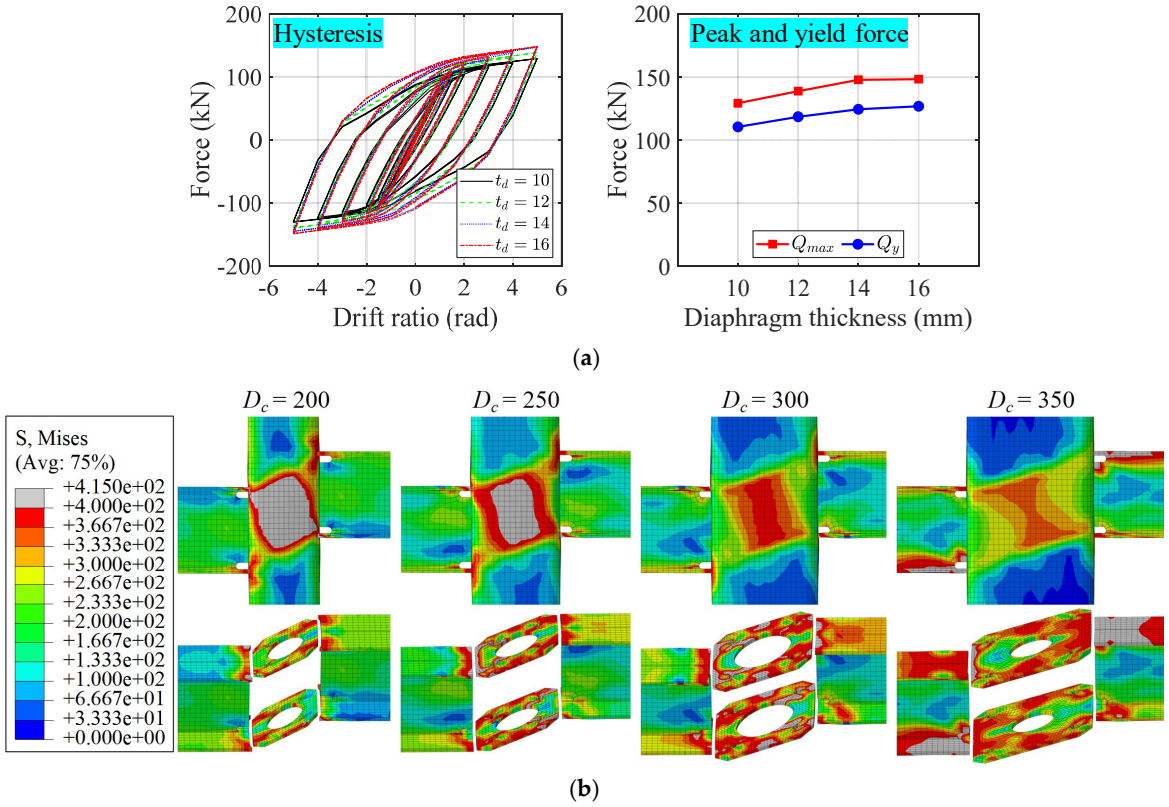

Figure 19. Influence of diaphragm thickness on SSB joints. (**a**) Force response of the joint, (**b**) stress distribution of the joint.

As the diaphragm thickness t_d increases, the hysteresis loops of both UDSB and SSB joints exhibit a progressive outward expansion, accompanied by stable increases in yield strength and peak load capacity. For all examined cases, the hysteresis loops remain relatively full without noticeable pinching, indicating that increasing the diaphragm thickness effectively enhances the stiffness and load-carrying capacity of the joint region. However, the rate of strength enhancement gradually decreases with further increases in diaphragm thickness, particularly when t_d exceeds 14 mm. Quantitatively, increasing the diaphragm thickness from 10 mm to 14 mm leads to an improvement in peak strength of approximately 10.5–14.4% for both UDSB and SSB joints.

Figures 18b and 19b present the equivalent von Mises stress distributions of the joints for different diaphragm thicknesses. When a relatively thin diaphragm is adopted (t_d = 10 mm), pronounced stress concentration develops throughout the diaphragm, with high stress levels extending across its entire section. As the diaphragm thickness increases, the degree of stress concentration within the diaphragm is progressively alleviated, and the stress distribution gradually shifts toward the joint panel zone and beam ends, resulting in a more uniform stress pattern. It is worth noting that previous experimental results showed that diaphragm fracture occurred at an inter-story drift ratio of approximately 3% when the diaphragm thickness was 12 mm, which is equal to the beam flange thickness. The present parametric analysis captures a similar tendency, as evident from the pronounced stress concentration observed in the diaphragm at this thickness, demonstrating good consistency between numerical and experimental observations.

Overall, diaphragm thickness is identified as a key structural parameter governing the mechanical performance of inclined-diaphragm irregular steel beam–CFST column joints. In essence, t_d controls the local stiffness and shear-resisting capacity of the diaphragm-assisted load-transfer path, and can therefore be regarded as a key detailing parameter of the proposed joint. Appropriately increasing the diaphragm thickness contributes to enhanced local load resistance and improved stress distribution; however, its effectiveness in further improving the overall joint capacity becomes marginal beyond a certain threshold. From a practical design perspective, the diaphragm thickness is recommended to be slightly greater than the beam flange thickness, so as to satisfy joint strength and ductility requirements while maintaining a reasonable balance between structural efficiency and material utilization.

4.7. Influence of Diaphragm Opening Diameter (R)

With all other geometric and material parameters kept constant, the diaphragm opening diameter was varied as R = 120, 140, 160, and 180 mm to conduct a parametric study on both UDSB and SSB joints. The corresponding force responses and stress distributions are presented in Figures 20 and 21, respectively.

Figures 20a and 21a illustrate the hysteretic responses as well as the variations in yield strength and peak strength under different opening diameters. It can be observed that, with increasing opening diameter R, the hysteresis loops of both UDSB and SSB joints gradually contract, accompanied by a continuous reduction in yield strength and peak load-carrying capacity. This trend indicates that enlarging the diaphragm opening reduces the effective load-resisting area and shear-transfer capacity of the diaphragm, which in turn leads to a decrease in the overall peak strength of the joint. Quantitatively, when the opening diameter increases from 120 mm to 180 mm, the peak strength decreases by approximately 11.6–13.0% for UDSB joints and about 18.9% for SSB joints.

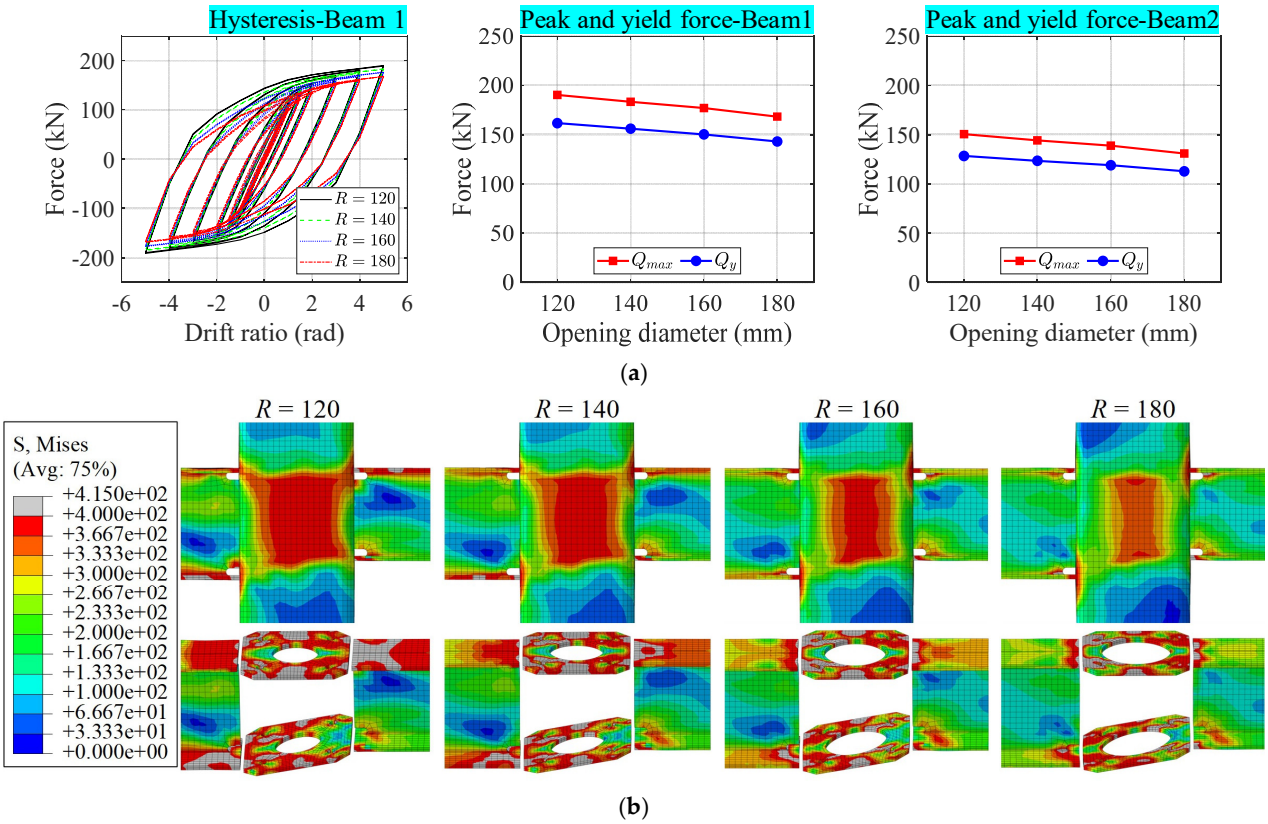

Figure 20. Influence of diaphragm opening diameter on UDSB joints. (**a**) Force response of the joint, (**b**) stress distribution of the joint.

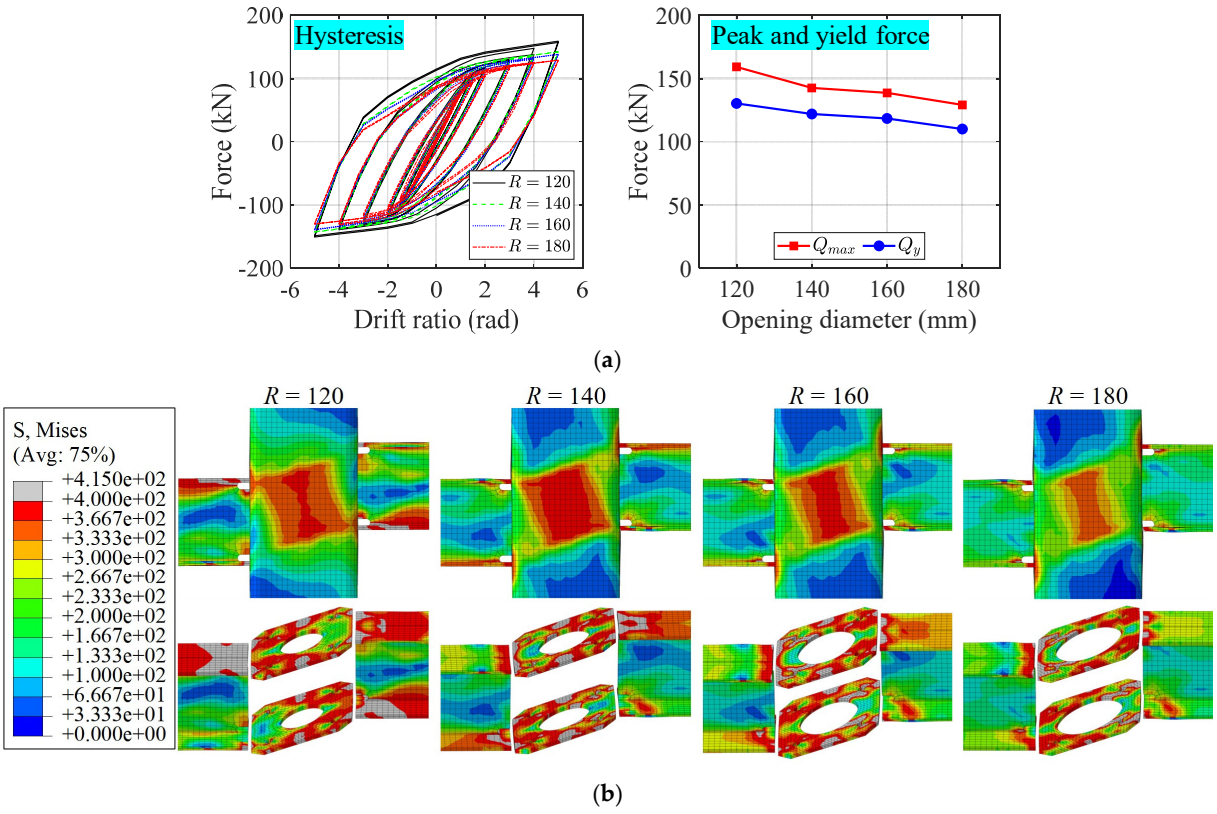

Figure 21. Influence of diaphragm opening diameter on SSB joints. (**a**) Force response of the joint, (**b**) stress distribution of the joint.

The equivalent stress distributions under different opening diameters are shown in Figures 20b and 21b. For smaller openings (R = 120 mm), stresses are relatively uniformly distributed among the beam ends, the joint panel zone, and the internal diaphragm, indicating effective participation of the diaphragm in shear transfer. As the opening diameter increases, pronounced stress concentrations develop around the edges of the diaphragm opening, while the stress levels in the joint panel zone and beam ends decrease accordingly. This does not indicate an improvement in joint behavior; rather, it reflects that the joint reaches its resistance limit under a lower external load level, while the remaining effective diaphragm material transfers the force through a reduced load path. This behavior demonstrates that the reduction in effective diaphragm area significantly impairs its shear-resisting contribution and alters the internal force transfer mechanism of the joint. Accordingly, the opening diameter mainly acts as a local detailing parameter that regulates the effectiveness of the diaphragm load path and the severity of stress concentration around the opening edges.

Overall, the diaphragm opening diameter is identified as a critical detailing parameter governing the load-carrying capacity of inclined-diaphragm irregular steel beam–CFST column joints. Excessively large openings markedly reduce joint strength and intensify local stress concentrations around the opening edges. From a practical design perspective, the diaphragm opening diameter should be carefully controlled to satisfy concrete casting and construction requirements while ensuring adequate mechanical performance and rational force transfer within the joint.

4.8. Influence of Axial Load Ratio (n)

Under otherwise identical geometric and material conditions, axial load ratios of n = 0, 0.15, 0.4, and 0.6 were considered to investigate their influence on inclined internal diaphragm joints. Given that UDSB and SSB joints exhibit similar mechanical response characteristics under axial compression, only the results of the SSB joints are presented herein. The corresponding force responses and stress distributions are shown in Figure 22.

Figure 22a illustrates the hysteretic responses of the joint together with the variations in yield strength and peak strength under different axial load ratios. It can be observed that, as the axial load ratio n increases, the overall shape of the hysteresis loops remains essentially unchanged, with no noticeable degradation in cyclic stability. In terms of load-carrying capacity, both the yield strength and peak strength exhibit only minor variations with increasing axial load ratio, remaining nearly constant within the investigated range, with differences limited to within 1%. These results indicate that, for joints with IIDs, the global load-carrying capacity is predominantly governed by the collaborative force-transfer mechanism among the beam, internal diaphragm, and column wall, while the influence of axial load ratio is of secondary importance. Within the investigated range, n therefore only has a limited effect on joint strength, compared with the geometric and diaphragm-related parameters discussed above.

Figure 22b presents the equivalent stress distributions of the joint under different axial load ratios. As the axial load ratio increases, the stress level in the column wall within the joint region is moderately elevated, indicating that axial compression amplifies the force demand on the column wall and promotes a more pronounced coupling between axial force and shear force within the joint region.

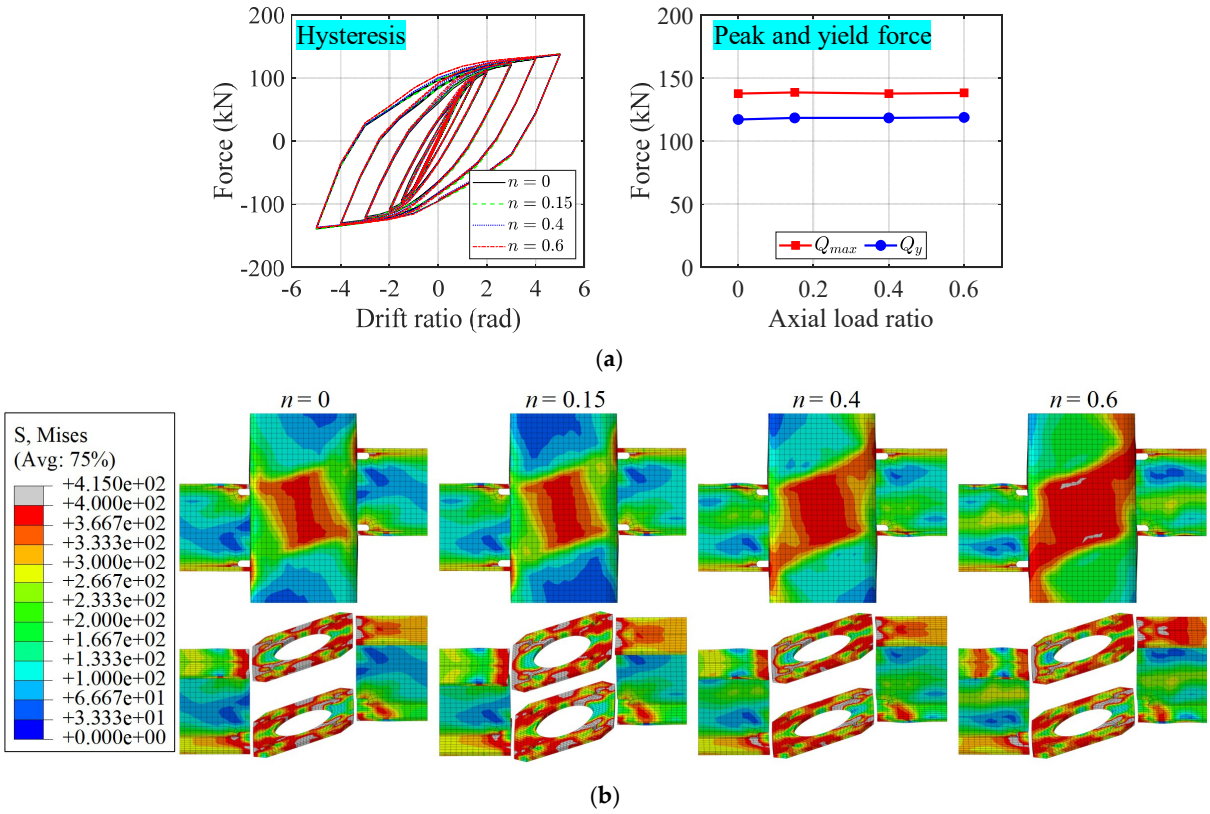

Figure 22. Influence of axial load ratio on SSB joints. (**a**) Force response of the joint, (**b**) stress distribution of the joint.

Overall, the axial load ratio has a limited influence on the hysteretic performance and load-carrying capacity of inclined internal diaphragm-type irregular steel beam–CFST column joints, but it can moderately increase the stress level in the column wall near the joint region. From an engineering design perspective, within the typical axial load ratio range encountered in high-rise buildings, axial load ratio does not constitute a governing parameter for joint strength. Nevertheless, under high axial compression levels, special attention should still be paid to potential local stress concentrations in the column wall and their implications for joint ductility and safety margins.

4.9. Discussion on Parameter Sensitivity and Governing Mechanisms

Based on the above parametric results, the investigated variables can be classified according to their mechanical roles and relative influence on joint behavior. For the UDSB joints, the beam depth ratio H_2/H_1 is the most influential parameter, because it directly governs the degree of force redistribution between the two beam sides and strongly affects the asymmetric development of joint resistance. As H_2/H_1 increases, a larger portion of the internal force is attracted to the deeper beam side, leading to a pronounced increase in the strength demand and stress concentration on that side, while the response of the shallower beam side is correspondingly suppressed.

The sectional parameters of the CFST column, namely the column wall thickness t_c and column width D_c, primarily control the stiffness and resistance of the joint panel zone. Increasing these parameters enhances the confinement and load-transfer capacity of the column face, reduces stress concentration in the panel zone, and promotes a more uniform stress distribution. Among them, increasing t_c provides a relatively direct strengthening effect, whereas the benefit of increasing D_c becomes less significant beyond a certain range, indicating a diminishing marginal contribution of column widening.

The diaphragm-related parameters, including the diaphragm thickness t_d and opening diameter R, mainly affect the efficiency of the diaphragm-assisted force-transfer path. Increasing t_d improves the local stiffness and shear-resisting capacity of the diaphragm, but its strengthening effect gradually becomes less pronounced once the diaphragm is sufficiently strong. By contrast, increasing the opening diameter R directly reduces the effective resisting area of the diaphragm and intensifies local stress concentration around the opening edges, resulting in a clear reduction in joint strength. Therefore, these two parameters can be regarded as key detailing variables for balancing strength enhancement and constructability.

Compared with the above parameters, the staggered floor ratio $\Delta H/H_1$ has a noticeable but moderate influence on the SSB joints within the investigated range. Its primary effect is to amplify geometric asymmetry and shift stress concentration toward the diaphragm–column wall connection, while the reduction in global strength remains limited. The axial load ratio n, on the other hand, shows only a minor influence on strength and hysteretic response under the present loading and parameter ranges, suggesting that the joint resistance is governed mainly by the local beam–diaphragm–column force-transfer mechanism rather than by axial compression in the column.

Overall, the present parametric study indicates that the governing parameters of inclined-diaphragm irregular steel beam-to-CFST column joints are not equally important. Parameters related to global geometric asymmetry and panel-zone resistance, such as H_2/H_1, t_c, and D_c, play a dominant role in controlling the overall joint response, whereas t_d and R mainly regulate the local effectiveness of the diaphragm load path. In contrast, $\Delta H/H_1$ and n have comparatively weaker influence within the investigated range. This distinction is useful for design, because it suggests that priority should be given to the control of beam depth ratio, column section parameters, and diaphragm detailing when proportioning this type of joint.

5. Design for Inclined-Diaphragm UDSB and SSB Connections

To establish a practical design method for inclined-diaphragm UDSB and SSB beam-to-CFST column joints, a theoretical investigation of the load transfer mechanism under beam flange tension is conducted based on the experimental and numerical studies presented above. In conjunction with the Chinese design specification (T/CECS 159-2004) [40], a mechanical model is developed to evaluate the flexural capacity of the joint, accounting for the inclination effect of the internal diaphragm and the strengthening contribution of the concrete infill in the joint panel zone. Based on the parametric study presented in Section 4, the present section is limited to strength-based calculation and design, with emphasis on joint yield strength, rather than force-displacement hysteretic behavior.

5.1. Load Transfer Mechanism and Theoretical Model

5.1.1. Column Face Yielding Mechanism

According to T/CECS 159-2004 [40], when tensile forces from the beam flange are transferred to the CFST column, a localized yielding mechanism may develop on the column face. The typical yield-line pattern is illustrated in Figure 23. Based on the principle of virtual work, the load corresponding to column face yielding can be expressed as,

$$P_c = \frac{(4x+2t_{bf})\left(M_{pc}+M_a\right)}{B_1} + \frac{4D_cM_p}{x} \quad (1)$$

where P_c is the tensile resistance associated with column face yielding; t_{bf} is the thickness of the beam flange.

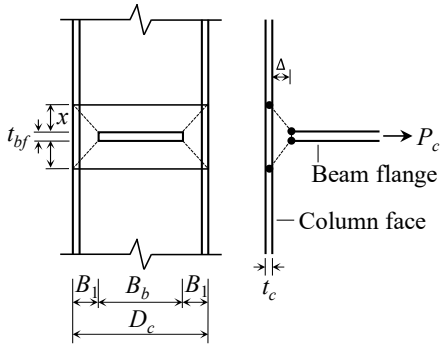

Figure 23. Yield-line mechanism of the CFST column face under beam flange tension.

M_{pc} denotes the yield bending moment per unit length of the column face, given by

$$M_{pc} = 0.25 f_{yc} {t_{cf}}^2 \tag{2}$$

in which f_{yc} is the yield strength of the steel tube column and t_{cf} is the column wall thickness. M_a represents the smaller bending resistance between the column-beam weld and the beam flange plate, defined as,

$$M_a = \min\left(M_p,\ 0.25 f_{wc} a^2\right) \tag{3}$$

where f_{wc} is the weld strength and a is the effective weld throat thickness. Considering the joint configuration adopted in this study, M_a is conservatively taken as M_{pc}. In addition, D_c is the width of the square steel tube column, and B_b is the width of the beam flange. The yield-line parameter x is obtained by solving $\partial P_c / \partial x = 0$, yielding,

$$x = \sqrt{B_1 D_c / 2} \tag{4}$$

5.1.2. Yield Mechanism of Internal Diaphragm with Opening

All the investigated joints are equipped with internal diaphragms containing ventilation openings. It is assumed that the yield line passes through the edge of the opening, as shown in Figure 24a. Neglecting the confinement effect of the concrete infill, the tensile resistance corresponding to yielding of the internal diaphragm can be expressed as,

$$P_{d1} = \sqrt{2} t_d f_{yd} (h_2 + h_1 / 2) \tag{5}$$

where P_{d1} is the tensile resistance of the internal diaphragm at yielding; t_d is the diaphragm thickness; f_{yd} is the yield strength of the diaphragm steel; h_1 is the clear distance between the ventilation opening and the diaphragm edge, and h_2 is the distance between the casting hole and the ventilation opening.

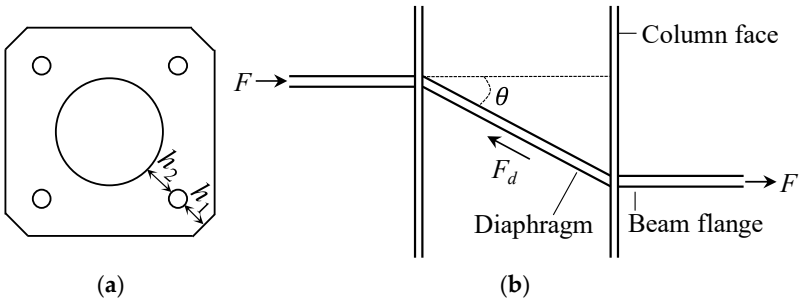

Figure 24. Geometry and force transfer mechanism of the inclined internal diaphragm (IID). (**a**) Geometry of the internal diaphragm, (**b**) force transfer mechanism of the IID.

Unlike conventional joints with horizontal diaphragms, the proposed joints adopt inclined internal diaphragms. Under beam flange tension, the relationship between the tensile force in the beam flange F and the force carried by the diaphragm F_d is illustrated in Figure 24b. Due to the inclination angle θ between the diaphragm and the beam flange, the force transfer path is no longer normal to the beam flange, resulting in a reduction in the effective load-carrying capacity of the diaphragm. Therefore, an inclination reduction factor $\cos\theta$ is introduced, and the effective tensile resistance of the inclined diaphragm is given by,

$$P_d = P_{d1}\cos\theta = \sqrt{2}\cos\theta t_d f_{yd}(h_2 + h_1/2) \quad (6)$$

This reduction formulation is consistent with the numerical observations presented earlier, where diaphragm inclination was found to reduce the joint strength.

It should be noted that, in addition to the effective horizontal component considered in Equation (6), the inclined diaphragm also introduces a vertical force component, which is transferred through the column face and panel zone. In the present simplified design model, this local effect is not treated as an independent diaphragm resistance term, but is considered to be implicitly associated with the column-face yielding mechanism discussed in Section 5.1.1.

5.2. Flexural Capacity of the Joint

Based on the above analysis, the tensile resistance at the beam flange level is jointly provided by the column face and the internal diaphragm. Taking the distance between the centerlines of the top and bottom beam flanges as the lever arm, the flexural capacity of the joint can be expressed as,

$$M_{b1} = (P_c + P_d)\left(h_b - t_{bf}\right) \quad (7)$$

Substituting the expressions of P_c and P_d yields,

$$M_{b1} = \left[\frac{(4x+2t_{bf})(M_{pc}+M_a)}{D_c - B_b} + \frac{4D_c M_{pc}}{x} + \sqrt{2}\cos\theta t_d f_{yd}(h_2 + h_1/2)\right](h_b - t_{bf}) \quad (8)$$

where h_b is the distance between the centrelines of the upper and lower beam flanges.

FE results indicate that tearing failure or plastic hinge formation may occur in the H-section beam near the column face welds. Therefore, the flexural capacity of the beam end should also be checked. For fully welded connections, the beam-end flexural resistance should satisfy,

$$M_{b2} \le \gamma_x W_{nx} f_y \quad (9)$$

where M_{b2} is the beam-end flexural capacity; γ_x is the plastic development coefficient of the section; W_{nx} is the net section modulus of the beam; and f_y is the design flexural strength of the steel. In the present study, γ_x was taken as 1.05 according to the relevant Chinese design specification [40] for H-section members bending about the major axis.

Accordingly, the joint flexural capacity is determined as,

$$M_b = \min(M_{b1}, M_{b2}) \quad (10)$$

5.3. Effect of Concrete Infill and Design Recommendation

The flexural capacities predicted by the above theoretical model are generally lower than those obtained from experiments and finite element simulations. This discrepancy primarily arises from the fact that the strengthening effect of the concrete infill in the joint core is not explicitly considered in the analytical model. As demonstrated in Section 3.4, the concrete infill significantly enhances the joint resistance.

To account for this effect, a unified amplification factor K_c is introduced to represent the contribution of the concrete infill to the joint flexural capacity. This factor is determined through regression analysis of experimental results, numerical simulations, and theoretical predictions. The flexural yielding capacity of the joint is finally expressed as,

$$M_y = K_c M_b \tag{11}$$

that is,

$$M_y = K_c \min\left(\begin{bmatrix} \left(\frac{(4x+2t_{bf})(M_{pc}+M_a)}{D_c - B_b} \right) + \left(\frac{4D_c M_{pc}}{x} \right) + \sqrt{2}\cos\theta t_d f_{yd}(h_2 + h_1/2) \end{bmatrix} (h_b - t_{bf}) \\ \gamma_x W_{nx} f_y \end{bmatrix} \right) \tag{12}$$

Based on the experimental results and parametric finite element analyses (FEA) of UDSB and SSB joints, the concrete amplification factor K_c is calibrated separately for the two joint types. As shown in Figure 25, the yield moment obtained from FEA (M_{FEA}) exhibits a linear correlation with those predicted by the proposed design equations without considering concrete infill (M_{Eq}). To evaluate the regression accuracy, the root mean square error (RMSE) was adopted, which is defined as,

$$\text{RMSE} = \sqrt{\frac{1}{n}\sum_{i=1}^{n}\left(M_{FEA,i} - M_{Eq,i}\right)^2} \tag{13}$$

where n is the number of data points included in the regression, $M_{FEA,i}$ is the yield moment obtained from the finite element analysis for the i-th joint case, and $M_{Eq,i}$ is the corresponding yield moment predicted by the calibrated design equation.

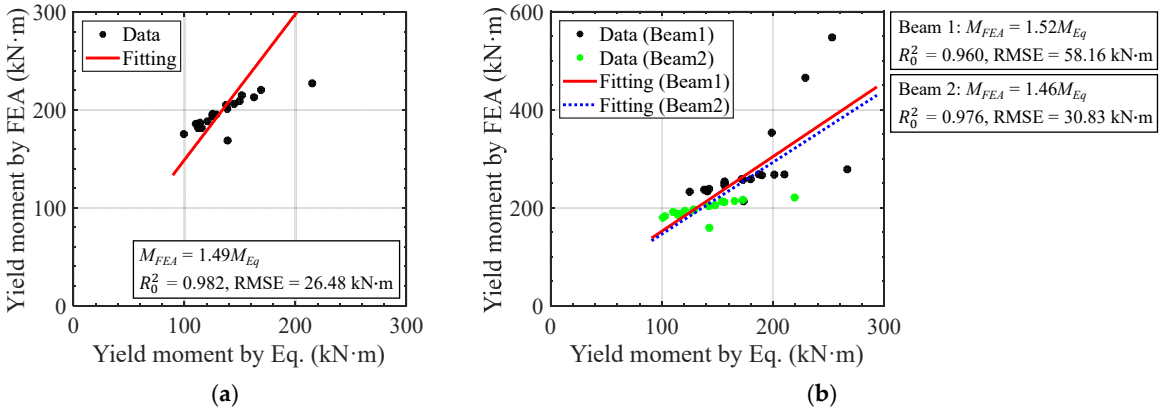

Figure 25. Regression of yield moment obtained from FEA and design equations. (**a**) UDSB joints, (**b**) SSB joints.

The regression results indicate that the calibrated amplification factors for the UDSB and SSB connections are very close, both being approximately 1.5. This observation suggests that, within the range of joint configurations and parameters investigated in this study, the contribution of the core concrete to the flexural yield capacity of inclined-diaphragm connections is comparable for UDSB and SSB joints, despite their different load transfer characteristics associated with the unequal-depth beam configuration and the stepped-beam arrangement. Accordingly, for practical design purposes, it is recommended that a unified value of K_c = 1.5 be adopted for inclined-diaphragm UDSB and SSB connections to account for the enhancement effect of the core concrete on the joint flexural capacity.

6. Limitations and Future Improvements

The validated FE models developed in this study can reasonably capture the pre-fracture global response, stress distribution, and force-transfer mechanism of inclined-diaphragm irregular steel beam-to-CFST column joints. Therefore, they provide a suitable basis for evaluating the effects of key geometric and detailing parameters on joint strength and for developing a strength-based design method.

Nevertheless, several limitations of the present study should be noted. First, although the improved constitutive model enhances the simulation of cyclic steel behavior, the FE model does not explicitly account for crack initiation, fracture propagation, or material separation in the diaphragm and welded regions. As a result, the numerical results are mainly applicable to the pre-fracture stage of joint behavior and are not intended to represent post-fracture strength degradation or residual response. Second, the parametric analysis focuses primarily on strength-related behavior, including yield strength, peak strength, and stress distribution. Response-based indices, such as force-displacement skeleton curves, moment-rotation hysteretic characteristics, stiffness degradation, and ductility evolution, were not systematically incorporated into the present analytical framework. Accordingly, the proposed method should be regarded mainly as a strength-oriented design approach. Third, the proposed design method was established based on the parameter ranges investigated in this study. Its applicability to joints with significantly different geometric configurations, material properties, welding details, or fracture-controlled failure modes requires further verification.

Future work will focus on extending the present study toward response-based design methods for this type of joint, particularly by incorporating force-displacement skeleton curves and hysteretic characteristics, to provide more comprehensive information for practical design and engineering applications.

7. Conclusions

This study investigated irregular steel beam–CFST column joints incorporating IIDs, including UDSB and SSB configurations. Based on previous full-scale cyclic loading tests, three-dimensional nonlinear FE models were developed and validated, followed by systematic parametric analyses and theoretical investigations. The seismic performance and load-resisting mechanisms of the connections were examined, and a corresponding design method was proposed. The main conclusions are summarized as follows:

(1) The FE models are capable of accurately predicting the hysteretic response, initial stiffness, and maximum strength of both UDSB and SSB joints. The discrepancies between numerical predictions and test results are within 5%. The models identify the same critical stress concentration regions observed in the experiments and reasonably capture the stress evolution process and failure modes prior to joint failure.

(2) IIDs significantly enhance the seismic performance of irregular steel beam–CFST column joints. Compared with joints without diaphragms, the introduction of inclined diaphragms increases the initial stiffness and load-carrying capacity by approximately 2.0–2.3 times and 1.16–1.8 times, respectively. The diaphragms effectively improve the force transfer path within the joint core and substantially alleviate local stress concentration in the column wall, making them a key structural measure governing joint strength.

(3) The concrete infill in the joint core provides stable enhancement to both stiffness and strength by increasing confinement and participating in shear force transfer. The presence of concrete infill increases the joint stiffness and strength by approximately 1.3 times and 1.2–1.3 times, respectively. Although its strengthening effect is less pronounced than that of the internal diaphragm, the contribution of concrete infill to

the overall joint capacity is non-negligible in cases governed by column face yielding and diaphragm action.

(4) Parametric analyses indicate that the beam depth ratio, staggered floor ratio, column wall thickness, column width, diaphragm thickness, and diaphragm opening diameter have significant influences on joint strength and stress distribution. Among these parameters, the column wall thickness, column width, and diaphragm detailing play a particularly important role in controlling the stress state within the joint core. In contrast, within the range investigated in this study, the axial load ratio has a relatively minor effect on the hysteretic behavior and load-carrying capacity of the joints.

(5) Based on the existing column face yielding theory and the proposed yield mechanism of inclined diaphragms with openings, a flexural strength prediction model applicable to UDSB and SSB connections was developed. By introducing a concrete amplification factor K_c, the strengthening effect of the concrete-filled joint core was incorporated into the design expression. Calibration based on experimental results and FEA shows that the K_c values for UDSB and SSB joints are close, clustering around 1.5.

Author Contributions: Conceptualization, P.L.; methodology, J.J.; software, J.J.; validation, P.L., Y.S., W.J. and T.G.; formal analysis, Y.S., W.J. and T.G.; investigation, Y.S., W.J. and T.G.; resources, Y.S., W.W., W.J. and T.G.; data curation, P.L. and J.J.; writing—original draft preparation, J.J.; writing—review and editing, P.L., J.J. and W.W.; visualization, J.J.; supervision, W.W.; project administration, P.L.; funding acquisition, P.L., J.J. and W.W. All authors have read and agreed to the published version of the manuscript.

Funding: This work was financially supported by the National Natural Science Foundation of China (NSFC) with Grant No. 52378182, the Shanghai Pujiang Program with Grant No. 25PJA145, and the Postdoctoral Fellowship Program of CPSF under Grant No. GZC20252127.

Data Availability Statement: The original contributions presented in the study are included in the article; further inquiries can be directed to the corresponding author.

Acknowledgments: The authors would like to express their sincere appreciation to all those who provided assistance during the experimental program.

Conflicts of Interest: Authors Peng Li and Weifeng Jiao were employed by the company China Construction First Group Corporation Limited. Author Yue Sheng was employed by the company Pinghu City Construction Investment Corporation Limited. The remaining authors declare that the research was conducted in the absence of any commercial or financial relationships that could be construed as a potential conflict of interest.

References

1. Thai, H.T. Beam-to-CFST column joints in steel-concrete composite buildings: A comprehensive review. *Structures* **2024**, *68*, 107123. [CrossRef]
2. Wahab, A.G.; Fang, W.; Tao, Z. Axial Compression behavior of L-shaped CFST columns enhanced by fully bolted threaded-rod confinement: An experimental assessment. *J. Compos. Sci.* **2026**, *10*, 77. [CrossRef]
3. Han, D.; Tao, Z.; Ghafar, W.A.; Hasan, M.M.; Xiao, W.; Wang, T.; Zhou, K.; Dai, H. Experimental study on the seismic performance of L-shaped CFST columns in different combinations. *Buildings* **2023**, *13*, 2320. [CrossRef]
4. Tao, Z.; Hasan, M.M.; Han, D.; Qin, Q.; Ghafar, W.A. Study of the axial compressive behaviour of cross-shaped CFST and ST columns with inner changes. *Buildings* **2023**, *13*, 423. [CrossRef]
5. Hasan, M.M.; Tao, Z.; Ghafar, W.A.; Huangfu, S.E.; Zhang, Z. Investigating the axial compressive behavior of cruciform CFST columns: An experimental study. *Structures* **2024**, *69*, 107538. [CrossRef]
6. Wahab, A.G.; Ye, J.; Tao, Z. Seismic performance of a novel replaceable shear-plate joint for special-shaped concrete-filled steel tube columns. *Thin-Walled Struct.* **2026**, *220*, 114344. [CrossRef]
7. Wahab, A.G.; Chen, L.; Tao, Z. Seismic performance of a novel beam-to-column connection for concrete-filled special-shaped steel tubular frames. *J. Constr. Steel Res.* **2026**, *242*, 110333. [CrossRef]

8. Kuwahara, S.; Kumano, T.; Inoue, K. The elasto-plastic behaviors of joint panels at the connection of rectangular steel column and two H-shaped beams with different depth. *J. Struct. Constr. Eng. AIJ* **2000**, *533*, 175–181. (In Japanese) [CrossRef]
9. Mou, B.; Bai, Y. Experimental investigation on shear behavior of steel beam-to-CFST column connections with irregular panel zone. *Eng. Struct.* **2018**, *168*, 487–504. [CrossRef]
10. Sui, W.; Wang, Z.; Li, X. Experimental performance of irregular PZs in CHS column H-shape beam steel frame. *J. Constr. Steel Res.* **2019**, *158*, 547–559. [CrossRef]
11. Nakao, M.; Osa, H. Study on beam-to-column connections of H-shaped steel strong-axis cruciform columns with unequal beam depths on both sides. In *Annual Report of Kanto Branch, Architectural Institute of Japan*; Kanto Branch, Architectural Institute of Japan: Tokyo, Japan, 1984; pp. 97–100. (In Japanese)
12. Nakao, M.; Osa, H. Research on the behavior of beam-to-column connection between beams of different depths. In *Summaries of Technical Papers of Annual Meeting, AIJ (Tokai)*; Architectural Institute of Japan: Tokyo, Japan, 1985; pp. 917–918. (In Japanese)
13. Tateyama, E.; Inoue, K.; Matsumura, H. Stiffness and moment capacity of H-shaped beam connected to RHS-column without diaphragm at its lower flange level. *J. Struct. Constr. Eng. AIJ* **1990**, *416*, 113–123. (In Japanese) [CrossRef]
14. Bayo, E.; Loureiro, A.; Lopez, M. Shear behaviour of trapezoidal column panels. I: Experiments and finite element modelling. *J. Constr. Steel Res.* **2015**, *108*, 60–69. [CrossRef]
15. Jordão, S.; Silva, L.S.; Simões, R. Behaviour of welded beam-to-column joints with beams of unequal depth. *J. Constr. Steel Res.* **2013**, *91*, 42–59. [CrossRef]
16. Hashemi, B.H.; Jazany, R.A. Study of connection detailing on SMRF seismic behavior for unequal beam depths. *J. Constr. Steel Res.* **2012**, *68*, 150–164. [CrossRef]
17. Xue, J.; Hu, Z.; Peng, X.; Liu, Z. Experimental study on failure mechanism of irregular joints between steel box columns and beams. *J. Build. Struct.* **2010**, *31*, 50–54. (In Chinese) [CrossRef]
18. Mou, B.; Li, X.; Bai, Y.; Wang, L. Shear behavior of panel zones in steel beam-to-column connections with unequal depth of outer annular stiffener. *J. Struct. Eng. ASCE* **2019**, *145*, 04018247. [CrossRef]
19. Mou, B.; Pang, L.; Qiao, Q.; Yang, Y. Experimental investigation of unequal-depth-beam-to-column joints with t-shape connector. *Eng. Struct.* **2018**, *174*, 663–674. [CrossRef]
20. Sui, W.; Zhang, Q.; Wang, Z. Cyclic behaviour of steel irregular tubular column panel zones. *Thin-Walled Struct.* **2020**, *154*, 106901. [CrossRef]
21. Jin, J.; Wang, W.; Jiao, W.; Sun, M.; Xu, H.; Tian, C. Seismic performance of an unequal-depth steel beam-to-CFST column joint with insert diaphragm: Experiment, numerical analysis and design method. *Thin-Walled Struct.* **2026**, *222*, 114508. [CrossRef]
22. Imai, K.; Yoshida, Y.; Saijo, M.; Watanabe, T.; Hirano, M. An experimental report on elasto-plastics behaviors of beam-to-column connections with an offset in right and left beam positions: Test specimens with right and left beam of same depth. *J. Struct. Constr. Eng. AIJ* **1991**, *425*, 27–35. (In Japanese) [CrossRef]
23. Kuwahara, S.; Kunitsugu, T. Experimental study on elasto-plastic behaviors of beam-to-column connection panel formed at intersection of one column and two offset beams fixed in parallel with each other. In *Summaries of Technical Papers of Annual Meeting, AIJ*; Architectural Institute of Japan: Tokyo, Japan, 2008; pp. 1031–1032. (In Japanese)
24. Liu, X.; Xu, C.; Peng, S.; Zhou, B. Influence of staggered floor and unequal height of left and right beam on seismic behavior of CFSST column-to-HSS beam composite frames. *J. Build. Eng.* **2023**, *66*, 105878. [CrossRef]
25. Liu, X.; Xu, C.; Peng, S.; Ni, T. Experimental study on seismic behavior of concrete filled square tubular frame with staggered beam-to-column joints. *Structures* **2021**, *29*, 286–293. [CrossRef]
26. Jin, J.; Nagae, T.; Chung, Y.L. Seismic and collapse behavior of existing high-rise steel buildings under long-period earthquakes. *J. Constr. Steel Res.* **2023**, *211*, 108151. [CrossRef]
27. Shi, G.; Zhang, N.; Bao, L.; Chen, X.; Zhou, F.; Jiang, S.; Zhao, H. Experimental investigation on local connection behaviour of thick-flange steel beam to CFST column joints under cyclic loadings. *Eng. Struct.* **2025**, *343*, 121206. [CrossRef]
28. Jin, J.; Chung, Y.L.; Nagae, T.; Yan, T.; Shigeta, E.; Lin, K.C. Post-earthquake repair of welded unreinforced flange-bolted web connections considering composite slab effects. *J. Constr. Steel Res.* **2024**, *221*, 108911. [CrossRef]
29. Jin, J.; Yan, T.; Nagae, T.; Chung, Y.L.; Ibarra, L.F. Seismic retrofit of H-section beam-to-HSS column connections in existing high-rise steel buildings. *J. Build. Eng.* **2025**, *111*, 113432. [CrossRef]
30. Li, P.; Jin, J.; Shi, C.; Wang, W.; Jiao, W. Experimental study on seismic behavior of irregular-shaped steel-beam-to-CFST column joints with inclined internal diaphragms. *Buildings* **2025**, *15*, 4514. [CrossRef]
31. *ANSI/AISC 341-22*; Seismic Provisions for Structural Steel Buildings. American Institute of Steel Construction: Chicago, IL, USA, 2022.
32. Dassault Systèmes Simulia Corp. *Abaqus 6.14 User's Manual*; Dassault Systèmes Simulia Corp.: Providence, RI, USA, 2014.
33. Feng, R.; Chen, Y.; He, K.; Wei, J.; Chen, B.; Zhang, X. Push-out tests of concrete-filled stainless steel SHS tubes. *J. Constr. Steel Res.* **2018**, *145*, 58–69. [CrossRef]
34. Han, L.H.; Xu, C.Y.; Tao, Z. Performance of concrete filled stainless steel tubular (CFSST) columns and joints: Summary of recent research. *J. Constr. Steel Res.* **2019**, *152*, 117–131. [CrossRef]

35. Xie, W.C.; Ye, Y. Finite element analysis and calculation method of concrete-filled stainless steel tubes under eccentric tension. *Buildings* **2023**, *13*, 2757. [CrossRef]
36. Yang, Q.; Zhao, B.; Liu, B.; Zhao, Z.; Mo, S. Influence of corrosion on loading capacity of circular concrete-filled steel tubular column. *J. Constr. Steel Res.* **2024**, *215*, 108564. [CrossRef]
37. Chaboche, J.L. Time-independent constitutive theories for cyclic plasticity. *Int. J. Plast.* **1986**, *2*, 149–188. [CrossRef]
38. Han, L.H.; Yao, G.H.; Tao, Z. Performance of concrete-filled thin-walled steel tubes under pure torsion. *Thin-Walled Struct.* **2007**, *45*, 24–36. [CrossRef]
39. Hai, L.; Wang, Y.; Ban, H.; Li, G.; Du, X. A simplified prediction method on Chaboche isotropic/kinematic hardening model parameters of structural steels. *J. Build. Eng.* **2023**, *68*, 106151. [CrossRef]
40. *T/CECS 159-2004*; Technical Specification for Structures with Concrete-Filled Rectangular Steel Tube Members. Chinese Planning Press: Beijing, China, 2004. (In Chinese)

Disclaimer/Publisher's Note: The statements, opinions and data contained in all publications are solely those of the individual author(s) and contributor(s) and not of MDPI and/or the editor(s). MDPI and/or the editor(s) disclaim responsibility for any injury to people or property resulting from any ideas, methods, instructions or products referred to in the content.